Connections between the Pacific Ocean Tropics and Midlatitudes on Decadal Timescales

DAVID W. PIERCE AND TIM P. BARNETT

Climate Research Division, Scripps Institution of Oceanography, La Jolla, California

MOJIB LATIF

Max Plank Institute for Meteorology, Hamburg, Germany

(Manuscript received 13 April 1998, in final form 28 May 1999)

ABSTRACT

Connections between the tropical and midlatitude Pacific on decadal timescales are examined using a 137-yr run of a fully coupled ocean–atmosphere general circulation model. It is shown that the model does a credible job of simulating both ENSO-scale and decadal-scale variability, and that there are statistically significant correlations between the midlatitudes and Tropics on decadal timescales. Three physical mechanisms linking the regions are examined: 1) Oceanic advection along isopycnal surfaces from the midlatitude subduction regions to the Tropics, 2) coastally trapped or Kelvin wave propagation between the Tropics and midlatitudes, and 3) near-simultaneous communication between the regions affected by changes in the atmosphere. It is found that communication via the atmosphere explains the strongest correlations found in the model. Further evidence is presented that is consistent with the idea that midlatitude sea surface temperature anomalies drive changes in the trade wind system that alter the east–west slope of the tropical thermocline, thereby effecting decadal-timescale changes in ENSO activity.

1. Introduction

Midlatitude Pacific sea surface temperature (SST) anomalies vary on decadal timescales (Namias 1969; Namias et al. 1988; Nitta and Yamada 1989; Trenberth 1990; Graham 1994; Trenberth and Hurrell 1994). This variability is important in human terms, as it is significantly correlated with wintertime weather variability over North America (Latif and Barnett 1994, 1996). Tropical Pacific variability associated with ENSO undergoes changes on decadal timescales as well (Wang 1995; Goddard and Graham 1997). This raises the obvious question of whether the decadal variability in these two regions is related.

In this paper we examine a 137-yr run of the ECHO-2 model (Frey et al. 1997; Venzke et al. 2000), a fully coupled, ocean–atmosphere general circulation model (O–AGCM). Our goal is to identify the physical mechanism causing the strongest interaction, on decadal timescales, between the tropical and midlatitude Pacific. Our use of the model in this context is to provide a surrogate dataset that is uniformly sampled in time and space over nearly a century and a half, a dataset that is not available from observations.

The question of midlatitude–tropical connections has been addressed by several studies, both theoretical and observational. The idea that tracers are injected onto isopycnal surfaces at the latitude of the wintertime outcrops (Stommel 1979), and that the thermocline is composed of these ventilated layers (Luyten et al. 1983), provides a theoretical context for the idea that the regions are connected by oceanic flow along isopycnals. The tritium studies of Fine et al. (1987) showed that such transport can be found in the real oceans; the details of the tracer field near the equator were shown to be consistent with the Sverdrup circulation by McPhaden and Fine (1988). Deser et al. (1996) traced observed North Pacific thermal anomalies along these isopycnal paths to at least 20°N, which raises the possibility that the climate of two regions might be connected by this mechanism [although Schneider et al. (1999) concluded that the response equatorward of 18°N is due to local forcing].

McCreary and Lu (1994) and Liu and Philander (1995), using ocean GCMs (OGCMs), illustrate several aspects of the three-dimensional tropical circulation, including model depictions of how subtropical wind stress influences the tropical thermal structure via the propa-

Corresponding author address: Dr. David W. Pierce, Scripps Institution of Oceanography, Climate Research Division, Mail Stop 0224, 9500 Gilman Drive, La Jolla, CA 92093-0224.
E-mail: dpierce@ucsd.edu

gation of anomalies along the ventilated isopycnals. Gu and Philander (1997) extended the isopycnal advection idea to a theory in which such anomalies play a key role in generating decadal-scale climate variability. Essentially, advection along isopycnals provides a decadal-scale delay, while amplification of advected thermal anomalies that reach the surface in the Tropics keeps the oscillations self-sustaining in the presence of noise and dissipation.

The idea of a tropical–midlatitude connection via wave propagation was addressed by Lysne et al. (1997), using an OGCM with climatological forcing in the Tropics and data assimilation in the midlatitudes. They identified a connection between the Tropics and midlatitudes effected by the westward propagation of midlatitude thermal anomalies as long Rossby waves to the western boundary, then equatorward propagation as coastal Kelvin waves. Connection via atmospheric processes has been examined by Alexander (1992), Trenberth and Hurrell (1994), Alexander and Deser (1995), Zhang et al. (1997), Miller et al. (1997), and Barnett et al. (1999), among others. These studies are frequently concerned with ENSO timescales rather than the decadal timescales of interest here, or they impose atmospheric conditions on the North Pacific rather than using a fully coupled system.

In this work we use data from the ECHO-2 model to test several of these ideas of how the midlatitudes and Tropics might be coupled on decadal timescales, including isopycnal advection, wave propagation, and atmospheric interaction. All these mechanisms have been suggested as important midlatitude–tropical linkages, and all are present to at least some degree in the ECHO-2 model. Our purpose is to determine which one is responsible for the strongest decadal timescale linkage when all are operating simultaneously in a fully coupled system that has both realistic ENSO variability and significant midlatitude decadal variability.

The paper is laid out as follows. Section 2 has a brief description of the ECHO-2 model (a more extensive characterization of the model's climatology is given in the appendix). In section 3 we describe the tropical and midlatitude Pacific variability in the ECHO-2 model, compare it to the available observations, and demonstrate that the model has significant correlations between activity in the midlatitude and tropical Pacific.

In sections 4, 5, and 6 we explore the ideas that the connection between the regions is accomplished by advection of thermal anomalies along isopycnals, wave propagation, and atmospheric connections, respectively. We find that atmospheric connections dominate in our solution. We discuss the results in section 7, including the questions of the direction of causality, and present our conclusions in section 8.

2. The ECHO-2 model

The ocean component of the ECHO-2 model is the Hamburg Ocean Primitive Equation (HOPE) ocean GCM, version 2.4, described by Wolff et al. (1997). The model has 20 vertical levels, half of which are in the upper 300 m. Horizontal discretization is on the Arakawa E grid, which is diamond shaped; therefore, a grid point's nearest neighbors are not along lines of constant lat–long, which should be kept in mind when considering the resolution. The width of the diamond is approximately 2.8° longitude; the height of the diamond is 0.5° lat between 10°N and 10°S, increasing smoothly to 2.8° lat poleward of 35°N or 35°S. Poleward of 60°, surface temperature and salinity are relaxed to observed climatology; otherwise, there are no flux correction terms. The atmospheric component is the Deutsches KlimaRechenZentrum climate model ECHAM4 (Roeckner et al. 1996), run at T42 resolution (approximately 2.8° lat $\times$ 2.8° long), with 19 layers in the vertical.

The ECHO-2 model is an improved version of ECHO-1 [used in Latif and Barnett (1994, 1996) and Schneider and Barnett (1997)], which coupled HOPE version 1 to ECHAM3. Compared to the earlier version, ECHO-2 has a more realistic Pacific equatorial cold tongue, greatly improved tropical ENSO variability, and a more realistic thermohaline circulation; these are result of changing the advection scheme to one with less numerical diffusion. Improvements in the atmospheric model lead to a more accurate simulation of the ITCZ, more realistic values of the surface heat flux budget in the tropical Pacific, and improvements in the precipitation field in the south Pacific convergence zone. A more complete description of the model's base climatology is presented in the appendix.

3. Characteristics of the model variability

We will first show that the Pacific tropical and midlatitude variability in ECHO-2 is similar to that observed and then demonstrate that there are significant correlations between the decadal variability in the two regions.

a. Tropical variability

Frey et al. (1997) describe the tropical Pacific characteristics of a 10-yr run of the ECHO-2 model. We will not repeat their analysis here, but merely note that the longer run we examine (137 yr) shows that even over multiple decades, the ECHO-2 model does a credible job of simulating ENSO-type warm and cold events in the tropical Pacific. Figure 1, for example, shows the leading empirical orthogonal function (EOF) of SST anomaly for the ECHO-2 model and from observations (da Silva et al. 1995). Both datasets have been filtered to remove variability with periods shorter than 2 yr or longer than 6 yr (i.e., to keep only ENSO-period variability). The area-weighted pattern correlation between the two EOFs is 0.79. Both model and observations show a strong tongue of variability in the tropical Pa-

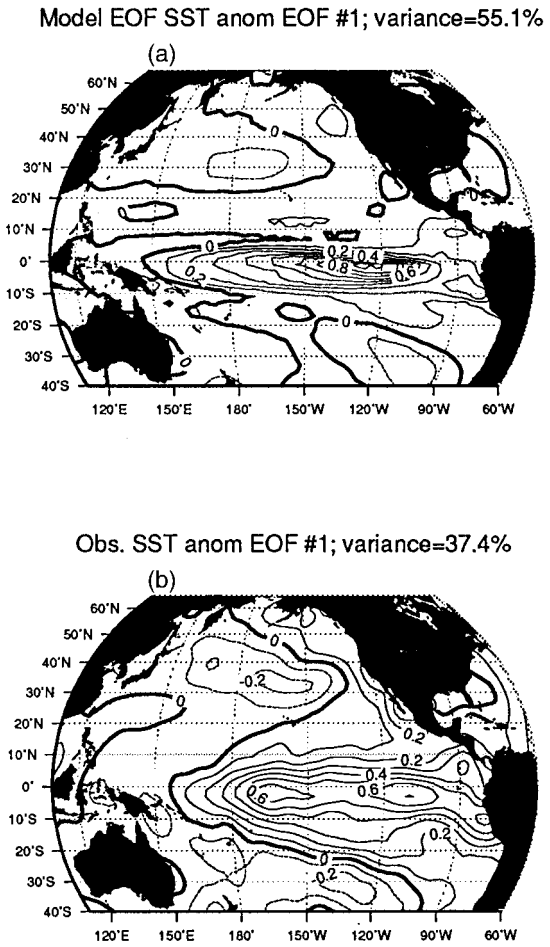

FIG. 1. Leading EOF of SST anomaly (a) for the ECHO-2 O–AGCM and (b) from observations. Data have been bandpass filtered to include periods between 2 and 6 yr. Units are °C, with the principal component normalized by its standard deviation.

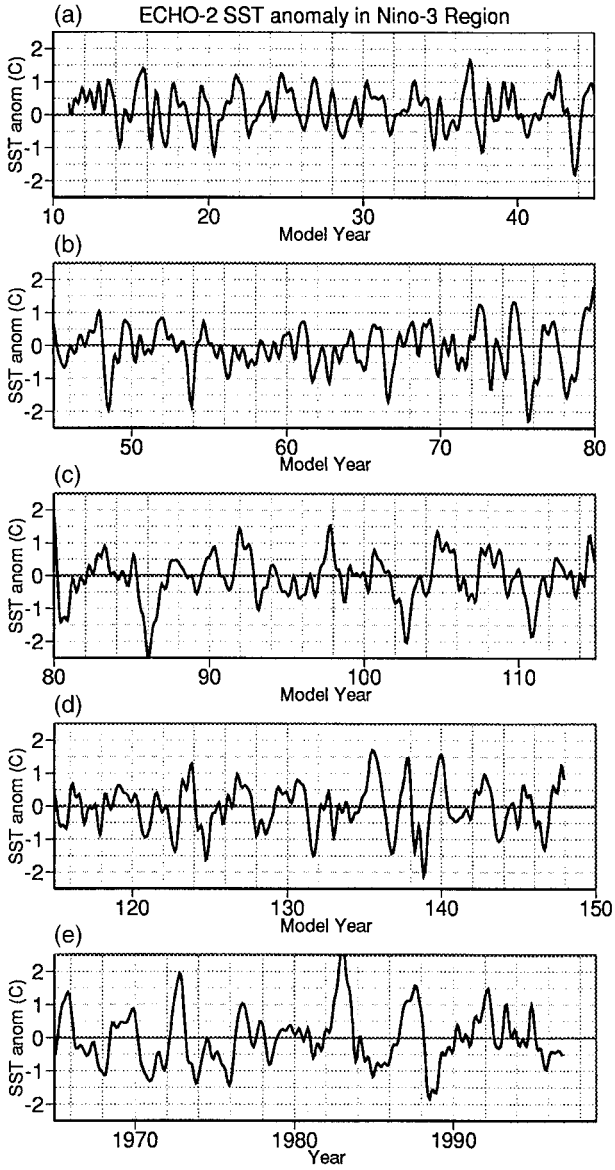

FIG. 2. (a)–(d) Time series of SST anomaly (°C) in the Niño-3 region for the ECHO-2 model and (e) from observations over the period 1965–95. The data have been filtered to remove periods shorter than 6 months.

cific, which arises from the warm and cold events of ENSO variability. One standard deviation of the temperature variability in the model (0.8°C) is comparable to that seen in the observations (0.7°C). Both model and observations show weak loading in the central North Pacific around 32°N, 170°W, and in the central South Pacific south of 20°S, although the loading in the model is weaker than in the observations in these areas. Compared to the observations, the model's variability is confined to a narrower band about the equator, a characteristic common to many coupled O–AGCMs (Mechoso et al. 1995). Additionally, it shows less activity along the west coast of North America than is observed, likely due to the model's inability to resolve coastally trapped waves, as discussed in section 5. This model deficiency should be kept in mind when evaluating the results of that section.

A time series of temperature anomaly in the model's Niño-3 region (90°–150°W) is shown in Fig. 2, along with observations from the period 1965–95 (e) for comparison. The amplitude of the events is reasonable, with peaks in the neighborhood of ±1.5° to ±2.0°C. The model also undergoes realistic variability in its ENSO cycles, with some periods (model years 15–50) consisting of more or less regular warm and cold events, other periods of relatively little activity (model year 55–72), and occasional bursts of strong events (such as model years 135–142). It is this ''modulation'' of the ENSO variability, and how it relates to activity in the midlatitudes, that is of interest here.

The spectrum of the Niño-3 SST variability is shown in Fig. 3 and confirms the visual impression from Fig. 2 that the model variability is characterized by slightly

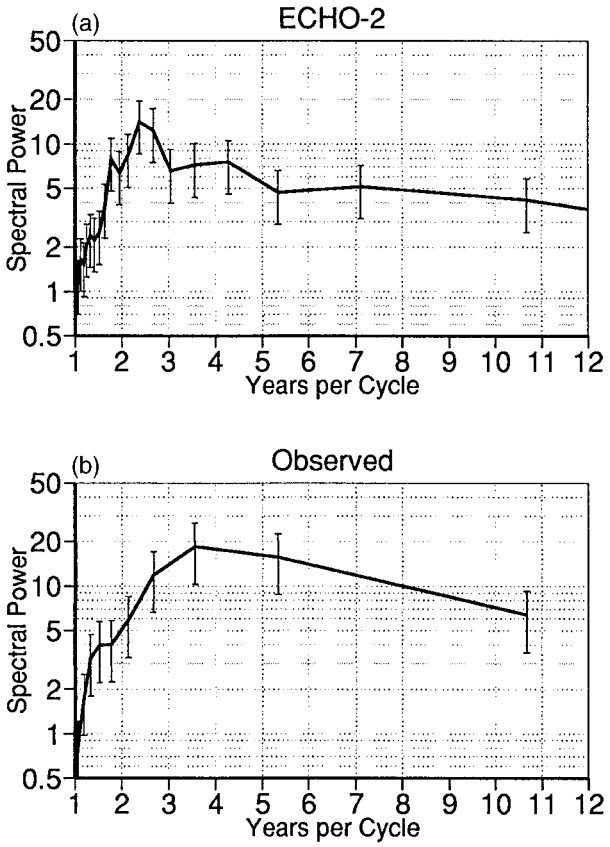

FIG. 3. (a) Spectrum of SST variability in the Niño-3 region from the ECHO-2 model and (b) observations.

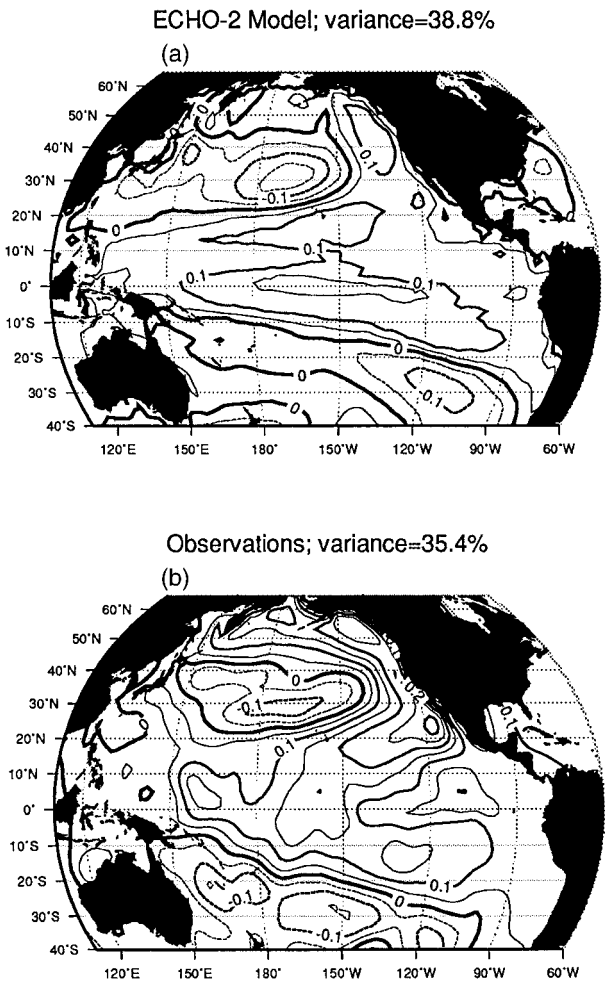

FIG. 4. Leading EOF of SST anomaly for data filtered to retain periods between 10 and 40 yr. Units are °C, with the principal component normalized by its standard deviation. (a) ECHO-2 model. (b) Observations.

shorter periods than the observations. The model spectrum has a sharper peak between 2 and 5 yr, while the observations have a (broad) peak between 3 and 6 yr. The observed spectrum also has a somewhat larger tail at periods out to 10 yr.

Overall, then, the ECHO-2 model does a credible job of simulating ENSO variability, with an amplitude similar to and a period only somewhat shorter than observed.

b. Decadal variability

Decadal variability in the Pacific, unlike the higher-frequency variability, is not confined to the Tropics but rather has significant expression in the midlatitudes. Figure 4, for example, shows the leading EOF of SST anomaly filtered to retain periods between 10 and 40 yr. The corresponding plot for observed data is also shown, using SST data over the period 1946–93 from da Silva et al. (1995) combined with National Meteorological Center (now the National Centers for Environmental Prediction) data from 1994 to 1997. The high-frequency cutoff of 10 yr $(\text{cycle})^{-1}$ was chosen to avoid any contamination by the El Niño band. The low-frequency cutoff of 40 yr $(\text{cycle})^{-1}$ was included to remove any possible contribution to the results from model drift or the effects of slow changes in the model's thermohaline circulation, which the 137-yr run is too short to fully resolve. The pattern correlation between the two EOFs is 0.56, with discrepancies in the North Pacific subpolar gyre and southwest Pacific contributing to a lower pattern correlation than that seen in the ENSO band. The model's inadequate representation of the subpolar gyre (discussed in the appendix) likely contributes to the errors in the EOF in that region, as might the poorly resolved coastally trapped waves (section 5). The reasons for the discrepancies in the southwest Pacific are not known.

In both the model and observations there is a pattern consisting of a negative region at about 30°N, 170°W around which wraps a horseshoe-shaped region of the opposite sign. The peak in the negative regions is similar for the model and observations; the explained variance is also similar between the two, with 38.8% for the

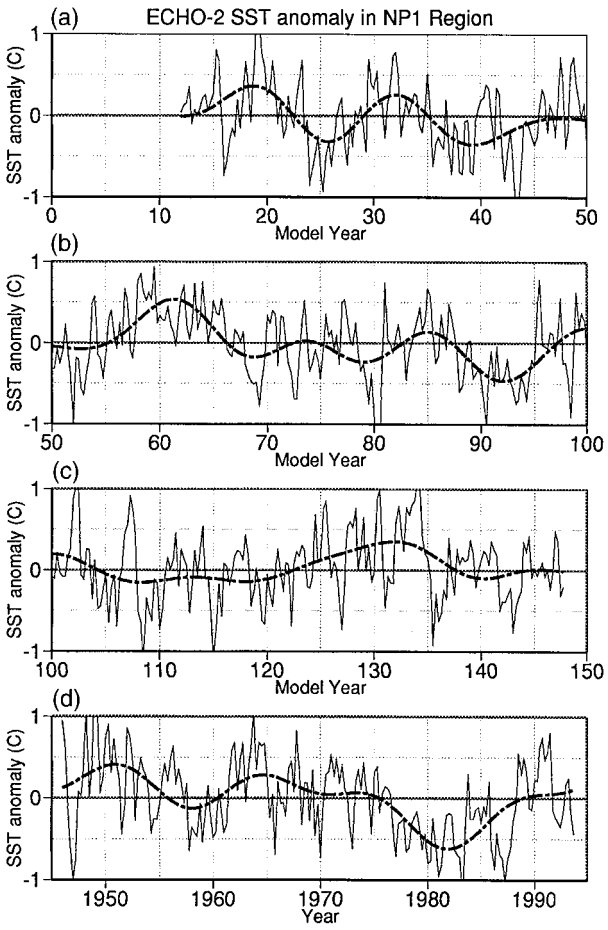

FIG. 5. Time series of seasonal SST anomaly (°C) in the region 25°–40°N, 180°–160°E for the (a)–(c) ECHO-2 model and (d) from observations over the period 1955–95. The broken line is the data filtered to remove periods shorter than 10 yr.

model and 35.4% for the observations. Zhang et al. (1997), using observed data and high-/low-pass filtering with a break at 6 yr (cycle)$^{-1}$ find a set of patterns similar to Figs. 1 and 4, and discuss the implications of the similarities of the patterns.

The EOF has a negative lobe in the Southern Hemisphere, making the overall effect roughly symmetric about the equator; however, this symmetry is more evident in the observations than in the model, where the negative loading becomes indistinct west of 150°W. The observations have more positive loading off the west coast of North America (about 0.3°C for the observations versus 0.15°C for the model).

The temporal character of the decadal SST variability in the model is shown in Fig. 5. Plotted is North Pacific SST anomaly averaged over the region 25°–40°N, 180°–160°W, where the central Pacific EOF reaches its maximum magnitude. Both raw seasonal anomalies and anomalies filtered to remove periods shorter than 10 yr are shown. The bottom panel of Fig. 5 shows the same data, from observations (da Silva et al. 1995), for comparison. Although the length of the observed time series is too short for detailed comparison, it can nevertheless be seen that the model variability is reminiscent of the observations. The decadal-scale fluctuations have a peak of about ±0.5°C in both the model and observations.

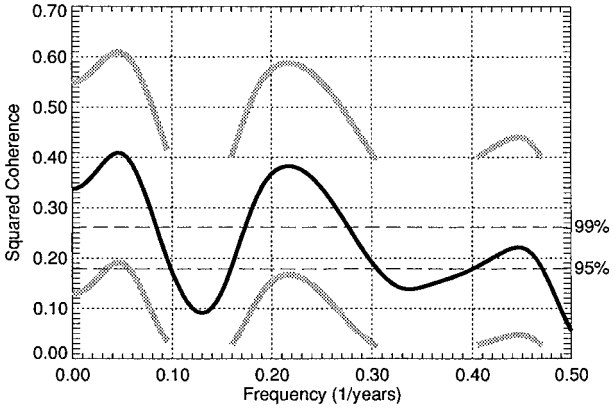

FIG. 6. Squared coherence between SST anomalies in the tropical and central North Pacific. The dashed lines show the levels of 95% and 99% significance, based on the null hypothesis of independent white noise; the gray lines show the 95% confidence limits.

c. Tropical/extratropical correlations

In this section we will demonstrate that there are correlations between longer timescale variability in the Tropics and extratropics in the ECHO-2 model. To begin with, note that the model and observed decadal SST EOFs (Fig. 4) show that there are regions of high loading in the central North Pacific, South Pacific, and Tropics. A cross-spectral analysis of SST anomalies in the centers of loading in the tropical (0°, 160°W) and North Pacific (35°N, 170°W) (Fig. 6) shows significant coherence in two frequency bands: 3–6 yr (the ENSO band) and 10+ yr (the decadal band), with a spectral gap between the two. Both peaks are significant at the 99% level. The phase relationship in the decadal band is not discernible from π radians; this indicates that SSTs in the equatorial and central North Pacific generally have an inverse relationship, but that any small phase shifts on top of this cannot be satisfactorily resolved by this technique. The origin and physics of the decadal peak in the cross spectrum are the subject of current research.

Time series of 10–40-yr bandpassed SST anomalies in the tropical, central North Pacific, and South Pacific regions of high EOF loading are shown in Fig. 7. The simple correlation between SST anomaly in the North and equatorial Pacific is −0.63; between the South and equatorial Pacific, −0.65. The correlations are significant at the 90% level (taking the number of degrees of freedom to be 6, based on the autocorrelation function). The correlation between the North Pacific and the equator is maximized at a lag of 0 yr; the correlation between the South Pacific and equator is maximized at a lag of

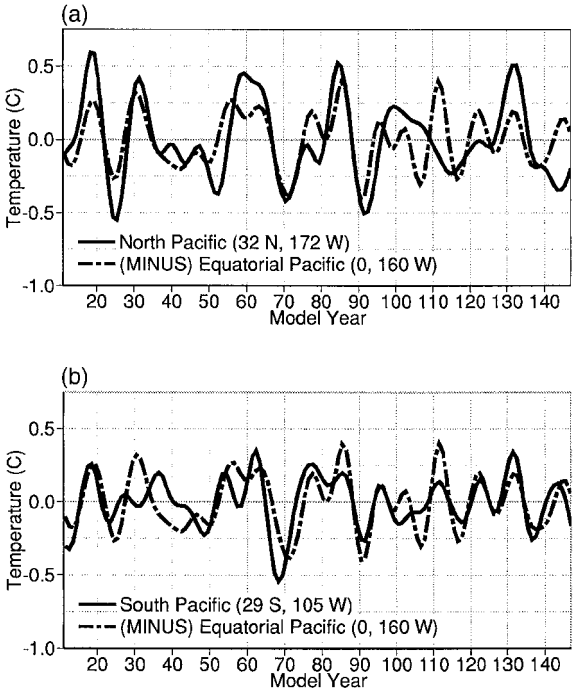

FIG. 7. Time series of 10–40-yr bandpassed SST anomalies (°C). (a) North Pacific (solid) compared to equatorial Pacific (dotted). (b) South Pacific (solid) compared to the same equatorial Pacific series (dotted). Note that the equatorial Pacific series has been multiplied by −1 to facilitate comparison.

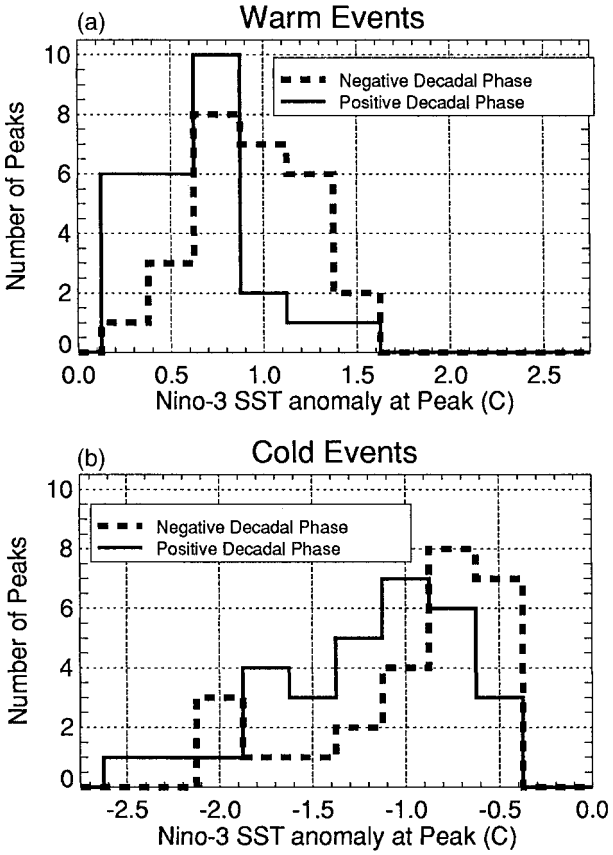

FIG. 8. Number of extrema in Niño-3 SST anomaly (vertical axis) as a function of the value at the extrema (horizontal axis), for both positive (dashed) and negative (solid) phases of the decadal variability. Bin size is 0.25°C.

1 yr, with the sense being that the South Pacific leads the equatorial Pacific. Using observations over the period 1945–93, the correlation is −0.68.

Considering first the North Pacific compared to equatorial Pacific (top panel), the two SST time series covary until model year 95, at which point the coherence between the two is abruptly lost (except, possibly, between model years 125 and 135). In the South Pacific Fig. 7b, the two series covary except for the period between model years 25 and 50. One possible explanation for this behavior is that there is a mechanism coupling the three regions on a decadal timescale that, however, does not act equally at all times in every locale. So, for example, during model years 11–20, 50–95, and 125–135, the SST anomaly in all three regions is changing with a fair degree of synchronicity. However, during years 20–50 the equatorial and North Pacific SST anomalies evolve together, while during years 95–145 the equatorial and South Pacific SST anomalies evolve together. The reason for this apparent nonstationarily in the relationship is the subject of current research.

The relationship between the model's El Niños and the decadal signal can be examined by comparing the amplitude of SST anomalies averaged over the Niño-3 region with an index of the Pacific decadal signal. For the decadal index we use the principal component (PC) of the EOF shown in Fig. 4. Figure 8 shows the probability distribution of peaks in Niño-3 SST anomaly as a function of the sign of this decadal index (positive values of the index indicate central North Pacific conditions warmer than average). Peaks are defined as local extrema in Niño-3 SST anomalies that have magnitude >0.25°C, and are either greater (for positive peaks) or less than (for negative peaks) all other values in an 20-month window, using 20-month low-pass filtered data. The window size of 20 months was selected as the decorrelation timescale on the basis of the autocorrelation function. There is a consistent shift such that the warm tropical events (El Niños) tend to be warmer during the negative phase of the decadal variability (cold in the central North Pacific), and some suggestion that cold events (La Niñas) tend to be colder during the positive phase of the decadal variability. A two-sample Kolmogorov–Smirnov test (Press et al. 1989) can be used to determine whether the distributions as a function of decadal phase are statistically different. The probability that the distributions for warm events are actually drawn from the same distribution is 0.03; for cold events, 0.12. Thus, the enhancement of El Niños when the central North Pacific is cold is a more consistent effect than

the enhancement of La Niñas when the central North Pacific is warm.

In summary, the ECHO-2 model shows statistically significant correlations between extratropical and tropical regions. This includes a relationship between cold decadal SST anomalies in the North Pacific and tropical Pacific warm events. However, this is subject to the qualification that there are extended periods when the relation between either the north or south extratropics and the equator is strong, and shorter intervals when the relationship is weak.

4. Propagation along isopycnals

The previous section demonstrated that the ECHO-2 model shows significant correlations between the midlatitude and Tropics. It could be imagined that one reason for this is that temperature anomalies are formed by air–sea interaction in the midlatitudes, then subduct and propagate westward and equatorward. Such propagation has been shown to occur in the North Pacific (Deser et al. 1996) and suggested as a important coupling mechanism for tropical–midlatitude climate variability (Gu and Philander 1997). However, in a recent, comprehensive study, Schneider et al. (1999) concluded that thermal anomalies south of 18°N arise from local forcing rather than the propagation of midlatitude anomalies. Nevertheless, we examine this mechanism here with the longer ECHO-2 time series, using analysis along isopycnal surfaces.

The procedure used was as follows. First, the three-dimensional density field was computed at each month. Then, the depths of selected isopycnals (σ = 22.0 to 28.0 by 0.5, then 29.0, 30.0, 32.0, 34.0, 37.0, 40.0, and 44.0) were calculated at every grid point and every month, using cubic spline interpolation between vertical levels. Temperature and salinity were subsequently projected onto the monthly isopycnal depths, again using cubic spline interpolation. Results on the σ = 25.5 and 26.0 isopycnals are shown here. These particular isopycnals were chosen for the analysis because they outcrop in the midlatitude region of interest. Unlike the other figures, Fig. 9 was computed using time-averaged rather than monthly isopycnals. This was done so that the effect of using time-averaged isopycnals could be determined. A direct comparison shows that using time-averaged rather than monthly isopycnals makes little difference.

Propagation of anomalies along time-averaged isopycnals can easily be discerned in the ECHO-2 run. For example, Fig. 9 shows a (positive) salinity anomaly moving along the σ = 26.0 isopycnal. The anomaly is first visible just south of the outcrop line, at about 32°N. It then propagates south and west, in agreement with ventilated thermocline theory (Luyten et al. 1983), reaching the western boundary at about 10°N [such behavior was described by Lu and McCreary (1995) as arising from a potential vorticity ''ridge'' associated with the intertropical convergence zone]. After that, the shear associated with the western boundary current makes the signal difficult to trace as a coherent entity, despite the fact that flow is toward the equatorial waveguide.

Examination of the entire run shows that this is typical behavior in the ECHO-2 model; most anomalies follow such a track to the western boundary. Anomalies that form farther to the west are more likely to head north after reaching the western boundary (as found in Gu and Philander 1997), while those forming farther east or south sometimes move south along the west coast of North America, then reach the equatorial regions directly. An illustration of this behavior is shown in Fig. 10. Shown is a sequence of lagged correlation maps of temperature anomaly on the 25.5 isopycnal, referenced to *two* time series: one in the North Pacific subduction region centered at 33°N, 138°W, and one in the South Pacific subduction region centered at 35°S, 90°W. (Contours from the two time series are overlaid on the same plot for conciseness but were computed independently.) The predominate behavior is for temperature anomalies to spread equatorward along the west coast of the Americas and then westward. In the Northern Hemisphere, two paths then become evident. 1) A tendency to travel almost directly west at 10°N, as seen in the salinity anomaly of Fig. 9. This signal then gets recirculated northward along the western boundary, as can be seen at year 10. 2) A tendency to spread farther south along the coast and enter the tropical region directly. The bottom left panel of Fig. 10 shows these two destinations most clearly. In the Southern Hemisphere, the anomaly moves directly toward the equator, but the correlation drops below 0.2 after 8 yr; all the contours at model year 10 are from the Northern Hemisphere source region.

Dissipation of the thermal anomalies during the transit from midlatitudes to Tropics (Fig. 11) was assessed by contouring the amplitude of thermal anomalies along the curved path they tend to follow, based on the data in Fig. 10. Although there were two large midlatitude thermal anomalies in model years 80–90 that rapidly extinguished, with virtually no information surviving to propagate to the Tropics, this was the exception rather than the rule. Near model years 35, 50–70, 100, and 130, thermal anomalies formed in the midlatitudes and propagated from 30° to 12°N with a diminution of amplitude typically less than 25%. This is consistent with the decrease in amplitude found in observed data (Schneider et al. 1999). We therefore conclude that the model does not unrealistically diffuse away information during this propagation.

The possibility for information to travel along isopycnals from the midlatitudes to the tropical regions having been demonstrated, it remains to examine whether this is a plausible mechanism for the tropical–midlatitude correlations shown in section 3. In this regard we will consider two questions: 1) are there phase shifts in activity between the Tropics and midlatitudes that are consistent with an isopycnal transport time of 7–10 yr,

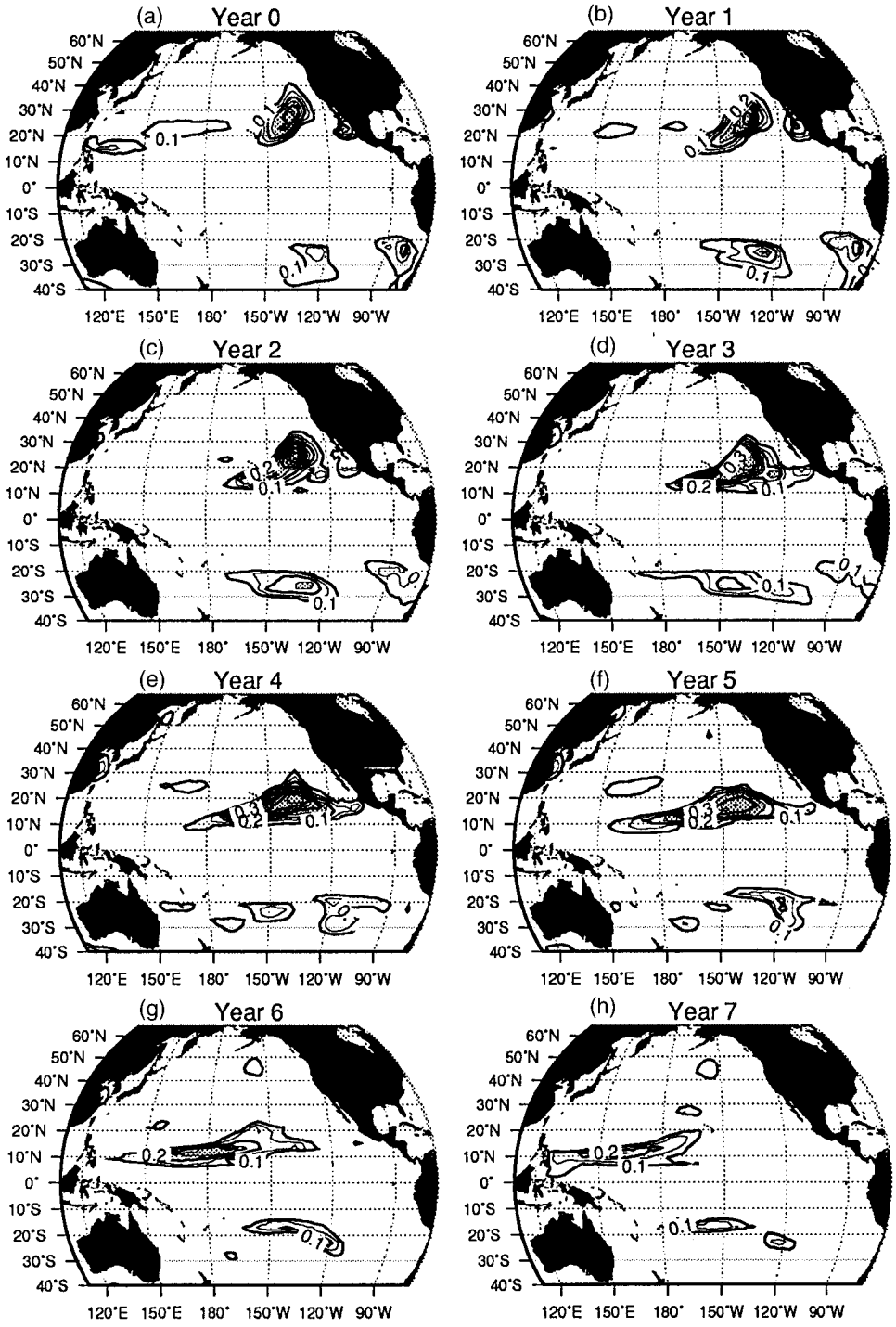

FIG. 9. (a)–(h) A sequence of contours of salinity anomaly (psu) on the $\sigma = 26.0$ isopycnal, with 1-yr lapse between frames.

as found here and in observations by Schneider et al. (1999)? 2) Is the amplitude of the transported signal sufficient to explain the variability?

Considering first the question of phase lags, Fig. 12 shows the lagged correlation between the curves of Fig. 7; the solid line is the lagged correlation between the North Pacific and the equatorial Pacific (top two curves of Fig. 7), and the dashed line is the lagged correlation between the South Pacific and equatorial Pacific (bottom two curves of Fig. 7). The North Pacific relation has its

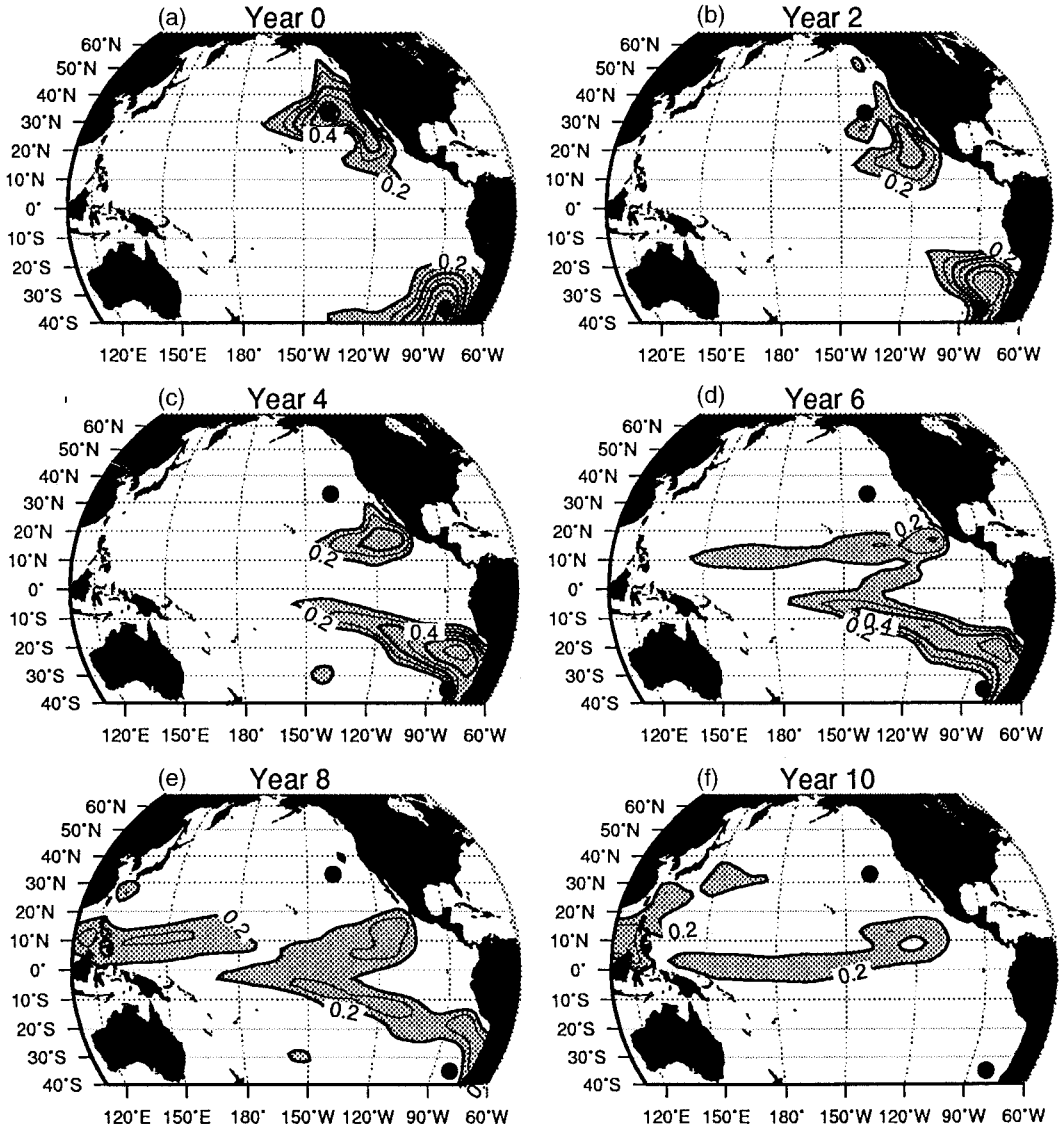

FIG. 10. (a)–(f) Lagged correlation maps of temperature anomaly on the $\sigma = 25.5$ isopycnal with two temperature anomaly time series (indicated by the dots): one at 33°N, 138°W, and one at 35°S, 90°W. There are two years between frames. Values greater than 0.2 are contoured, with an interval of 0.1. The Northern and Southern Hemisphere calculations were done separately but are shown here on the same maps for conciseness.

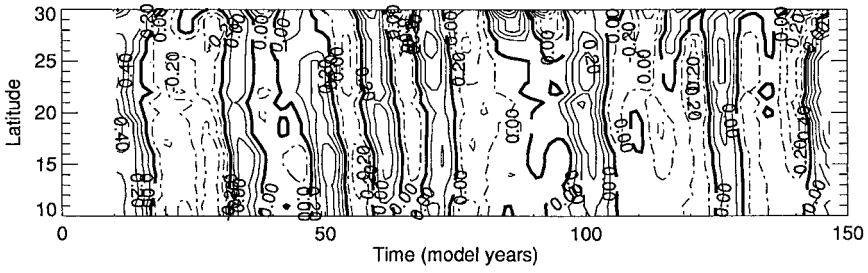

FIG. 11. Contours of temperature (°C) along the 25.5 isopycnal, as a function of model year, along the curved path that such anomalies tend to follow in moving from the midlatitudes to the Tropics. Contour interval is 0.1°C.

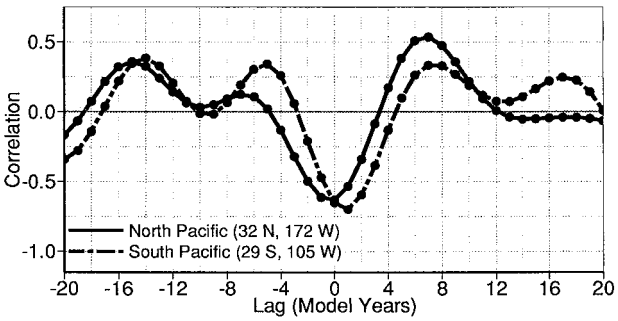

FIG. 12. Lagged correlation between North Pacific (33°N, 138°W) and equatorial (0°, 160°W) SST anomalies (solid), and South Pacific (29°S, 105°W) and equatorial (0°, 160°W) SST anomalies (dashed). Positive lags mean the midlatitudes lead the Tropics.

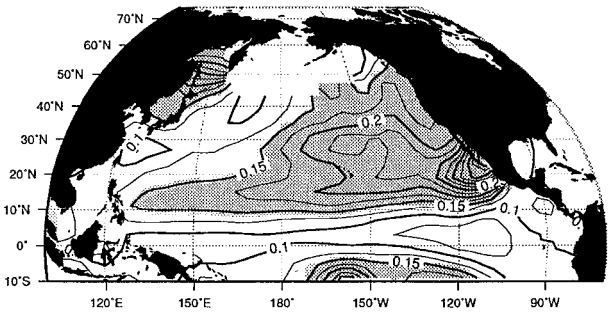

FIG. 13. Standard deviation (°C) of temperature anomalies along the depth-averaged $\sigma = 25.0$ isopycnal.

extrema at a lag of 0 yr, with a value of -0.63. Note that there is a lesser, marginally significant peak (0.53) at a shift of 7 yr, which suggests that isopycnal advection may be having some influence in the Northern Hemisphere, although at a weaker level than the process effecting the simultaneous correlation. This lesser peak was further examined by computing the lagged correlation between the same North Pacific SST index and the full three-dimensional temperature field, at lags of -20 to $+20$ yr. These fields showed no evidence that a region of positive correlation, representing the signature of an advected thermal anomaly, propagates beneath the surface from the midlatitudes to the Tropics and subsequently upwells. It appears instead to be a surface phenomena and is currently being investigated.

The Southern Hemisphere has its extrema at a lag of 1 yr (such that the South Pacific leads the Tropics), with a value of -0.70. The peak at a shift of 7 yr in this hemisphere is only 0.33 and is not significant. The lagged surface correlations, then, show that the strongest linkage between the (northern and southern) midlatitudes and tropical Pacific SSTs on the 10–40-yr timescale occurs with a delay of no more than one year, which rules out advection along isopycnals for this mechanism.

Considering now the question of the amplitude of the transported anomaly, Fig. 13 shows the standard deviation of 10–40-yr bandpassed temperature anomalies on the $\sigma = 25.0$ isopycnal. Only the Northern Hemisphere is shown, given the discussion above. The general impression is consistent with the propagation of anomalies as previously described, with lines of constant standard deviation roughly coinciding with the northeast to southwest track of advected anomalies. Note, however, that values drop rapidly once south of 10°N, reaching a minimum of less than 0.05°C on the equator. One possible explanation for this is that anomalies that enter the western boundary current system lose their amplitude due to shear-induced mixing. Examination of individual time series along advection paths on the isopycnal (not shown) confirms this time-independent view; that is, the amplitude of individual anomalies drops by a factor of 2 to 4 between 10°N and the equator.

The small amplitude of advected anomalies by the time they reach the Tropics (a two-standard-deviation signal would be in the range of 0.1°–0.2°C) suggests that it would be difficult for them to have a strong effect on the evolution of tropical winds. Balanced against this is the fact that the wind response in the Tropics tends to amplify initial perturbations, but there is no observational evidence to suggest that such small temperature signals would have a discernible wind response.

In sum, the ECHO-2 model shows that the strongest link between midlatitudes and tropics occurs with a delay of no more than one year. This rules out advection along isopycnals being a cause of decadal modulation of the ENSO cycle.

5. Connections via wave propagation

It is known from observations that at subannual frequencies, the Tropics and midlatitudes are linked along the eastern boundary by the propagation of coastally trapped Kelvin waves, which travel from the Tropics to the midlatitudes with phase speeds of 0.6–1.0 m s^{-1} (Enfield and Allen 1980). Additionally, evidence from OGCMs suggest that similar signals can travel from the midlatitudes to the Tropics along the western boundary in the North Pacific (Lysne et al. 1997). We consider here whether either of these mechanisms can explain the decadal correlations found in ECHO-2.

a. Poleward propagating coastally trapped waves

The model does, in fact, have an analog to poleward propagating coastally trapped waves. The top four panels of Fig. 14 shows the propagation of these, expressed as positive values of lagged correlation of basinwide sea surface height (SSH) anomaly with respect to an SSH time series centered on the equator at 110°W. There are two months between each frame. Figure 14 is based on monthly values high-pass filtered to retain only periods shorter than 3 yr; the motivation for this is to isolate the signal of interest, known from the observations to be relatively high frequency. Note that even the rela-

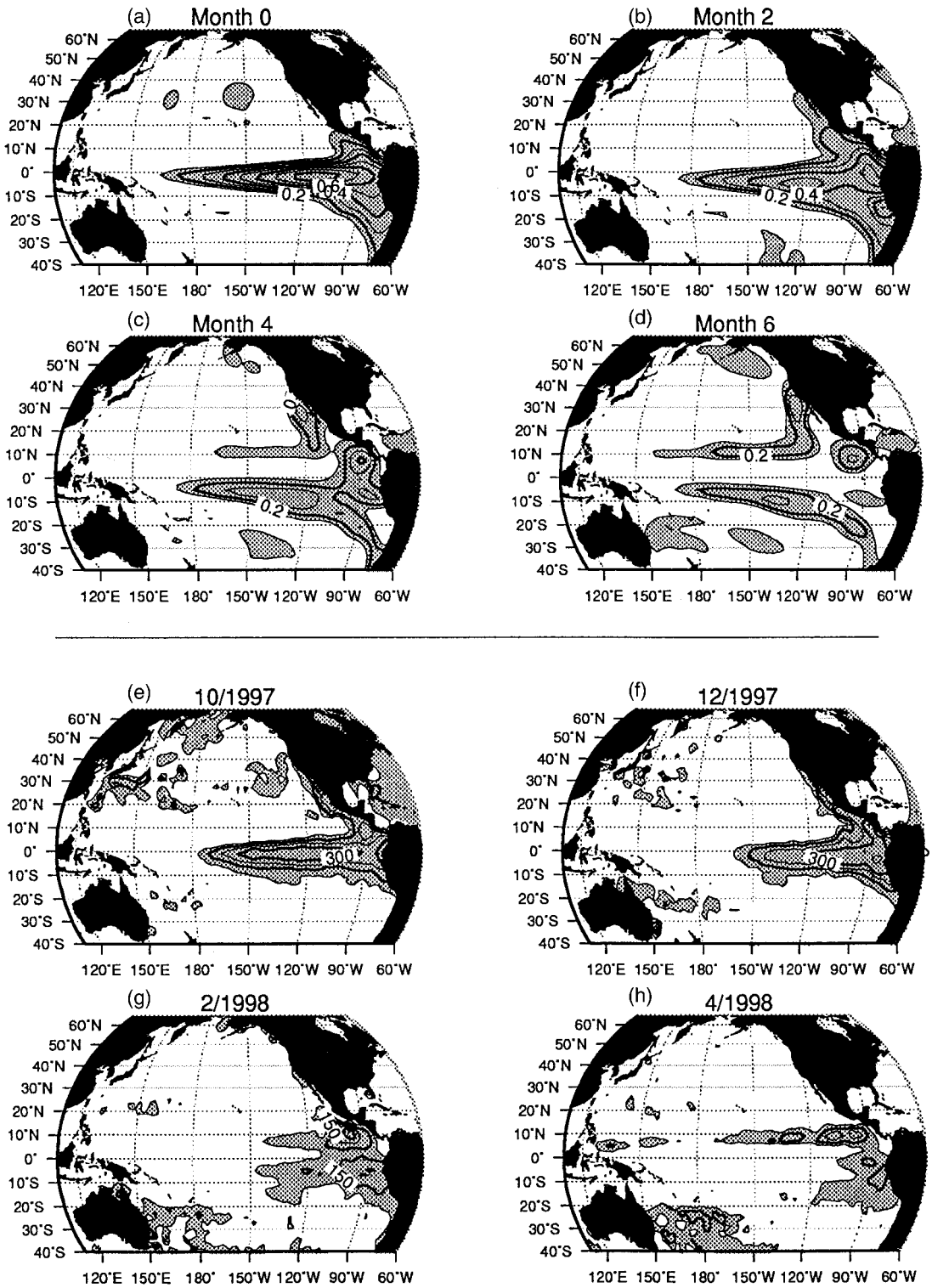

FIG. 14. (a)–(d): Lagged correlation between a time series of SSH anomaly centered on the equator at 110°W and subsequent SSH anomalies. There are two months between each panel. Only positive values are shown. (e)–(h): SSH anomalies from observations during an El Niño episode.

tively weak correlations shown in Fig. 14 are significant, because of the large degrees of freedom (monthly data, and an autocorrelation timescale of 5 months, give ~200 degrees of freedom). The lower four panels of Fig. 14 show positive values of sea surface height anomaly as measured by TOPEX/Poseidon, starting in October 1997 during a strong warm event. Note that these are not lagged correlations, as in the upper four panels, but rather sea surface height anomalies (mm) evolving during a particular warm episode.

During the months shown in Fig. 14, initial SSH anomalies in the tropical Pacific can be seen to propagate poleward along the west coast of the Americas. In the Northern Hemisphere, the signal reaches 32°N after 2 months; by 4 months, 40°N; and by 6 months, the Gulf of Alaska. The speed of propagation in the model is 0.4–0.6 m s^{-1}, distinctly slower than observed (Enfield and Allen 1980). Note how in the observed panel 4/1998 in Fig. 14, the signal appears to have completed its propagation along the west coast of North America, while the model still has a west coast signal clearly visible after six months.

In both the model and the particular observed event illustrated in Fig. 14, the propagating signal moves rapidly westward at about 10°N after four months. In the model this signal is roughly symmetric about the equator. Less symmetry can be seen in the observations, where the northern expression dominates. Whether this disagreement is due to a problem in the model or due to variability between different warm events is not known.

The fact that ECHO-2 has anything resembling the coastally trapped waves might be considered surprising, since the length scale of such waves is about 50 km (Gill 1982), and the distance between model grid points is generally over 100 km. Obviously, the waves are not going to be reproduced in detail, and from Fig. 14 it can be seen that the width of the propagating signal is much wider than 50 km.

Although the model has an analog to coastally trapped waves, this signal contains no expression in SST anomaly. Lagged correlations analogous to Fig. 14 for SST (not shown) have no sign of a concomitant SST signal that propagates in a fashion similar to the SSH signal. Therefore, the data do not support the idea that correlations in SST between the Tropics and midlatitudes are accomplished via this mechanism.

b. Equatorward propagating Kelvin waves

Lysne et al. (1997, hereafter LCG), using an OGCM assimilating data in the extratropical regions, found evidence that central North Pacific thermal anomalies propagate westward as long Rossby waves, then equatorward as coastal Kelvin waves, and then along the equator as Kelvin waves. Indices of heat storage anomalies (their Fig. 1) showed evidence of a feature propagating from the midlatitude Pacific to the equatorial Pacific with a timescale of 4–5 yr, distinctly faster than the isopycnal transport timescale of ~10 yr.

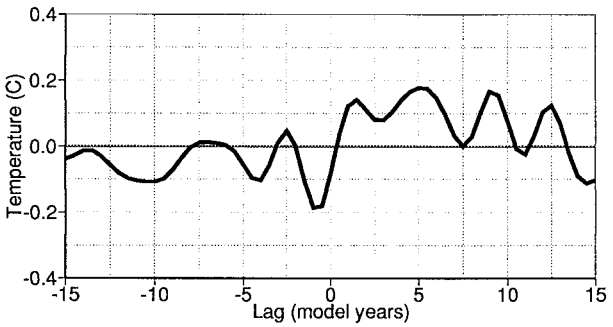

FIG. 15. Lagged correlation (model years) between heat content anomaly in the North Pacific and eastern equatorial region. Positive values indicate that the North Pacific leads the Tropics.

This mechanism does not seem to be strongly active in the ECHO-2 run. Figure 15 shows the lagged correlation coefficient between time series of heat content anomaly in the North Pacific (20°–40°N, 170°–145W) and the eastern equatorial region (5°S–5°N, 180°–80°W), both taken to a depth of 370 m and filtered to remove periods less than 3 yr (as per LCG). The structure is asymmetric, such that positive (negative) lags have positive (negative) correlations, with a broad peak at around +5 yr. This suggests that thermal anomalies do indeed propagate from the North Pacific to the Tropics. However, the magnitude of the correlation (<0.20) is not statistically significant.

These results might differ from those in LCG because of model factors, such as different OGCM characteristics or the longer run used here (137 vs 38 yr). The differences might also be due to the degradation of a propagating signal by tropical variability, since LCG intentionally used only climatological forcing in the Tropics, while ECHO-2 produces realistic variability in the region (section 3). LCG note that their results suggest that processes not related to advection from the midlatitudes can have an important effect on tropical warming/cooling as well, a finding consistent with the results shown here and in Schneider et al. (1999).

In summary, while ECHO-2 shows some evidence for wave propagation both from the Tropics to the midlatitudes and vice versa, neither appears to be causing the statistically significant correlations shown in section 3. The small horizontal scale of, for example, coastally trapped waves (~50 km) compared the model's resolution (~100 km) suggests that they can be represented only with distortion; in fact, they are found to have a propagation speed only one-half that observed. This does not change our conclusions—that the model's wave processes, albeit poorly represented, are *not* causing the model's demonstrated connections between the Tropics and midlatitudes—but does leave open the possibility that such waves might play additional roles in the real ocean. The ECHO-2 model is a tool that should be used

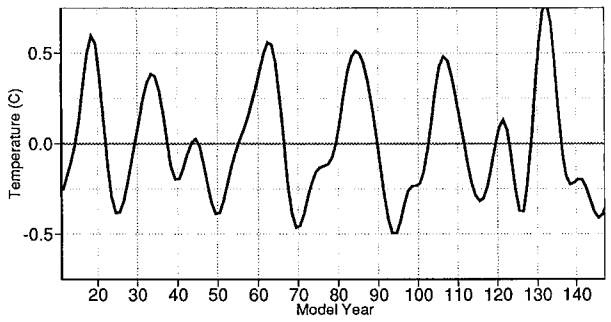

FIG. 16. Difference in SST between points in the North Pacific at 40°N, 170°W, and 20°N, 170°W. Data have been 10–40 yr bandpassed.

to examine larger-scale phenomena, one of which is considered in the next section.

6. Midlatitude/tropical connections via the atmosphere

As the discussion in section 4 pointed out, SST time series do not show any appreciable time lag between the tropical and midlatitude variability in the ECHO-2 model (Fig. 7). This suggests that the atmosphere mediates the response between the Tropics and extratropics on decadal timescales, rather than such a link being accomplished by oceanic transport. In this section we explore this possibility and show that such an interpretation is consistent with the ECHO-2 dataset.

There are well-known atmospheric links between the Tropics and midlatitudes on ENSO timescales (e.g., Horel and Wallace 1981; Blackmon et al. 1983; Alexander 1992), but less work has examined the issue on decadal or interdecadal timescales (Trenberth 1990; Trenberth and Hurrell 1994). No doubt this is partly because of the relatively short observational record; Pacific basinwide SST and wind stress datasets include only a few realizations of a decadal event. Thus, the 137-yr ECHO-2 dataset can play a valuable role in diagnosing this kind of relation.

To begin with, we note that ECHO-2 has a repetitive cycle of ocean–atmosphere interaction in the North Pacific similar to that described in Latif and Barnett (1994, 1996). This can be demonstrated in a number of ways; here we show a series of lagged correlation maps between an index of North Pacific SST anomaly variability and the zonal wind stress, τ^x. The index we take is the difference in SST anomaly between a box in the North Pacific centered at 40°N, 170°W, and a box centered at 20°N, 170°W (shown in Fig. 16). We chose to use this simple index rather than the PC of a basinwide EOF so that it would be clear that the correlations are locally valid in the North Pacific. The motivation for choosing τ^x will be discussed further below.

Figure 17 shows the correlation between the SST index and τ^x at various lags over a 10-yr period, during which time the state of the North Pacific climate system reverses. In the first figure of the sequence (top left), the sense of the cycle is such that there is anomalously

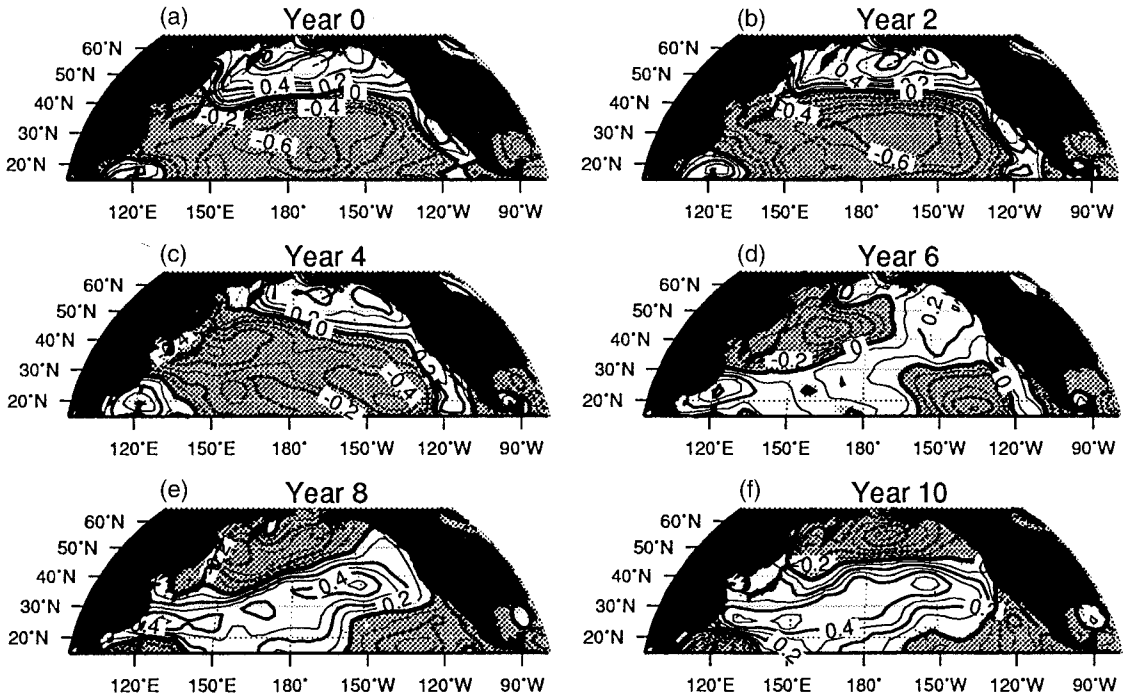

FIG. 17. Correlation maps between a North Pacific SST index and τ^x, lagged by various years to cover a 10-yr half-cycle. There are 2 yr between frames. Contour interval is 0.1; negative values are shaded.

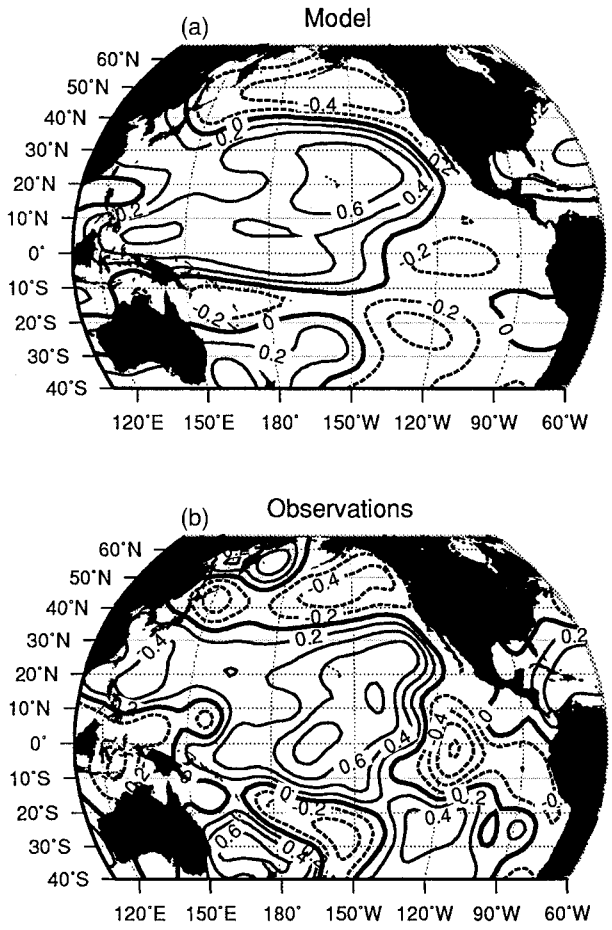

FIG. 18. Correlation between the leading PC of DJF North Pacific SST anomaly and τ^x. For the (a) model and (b) observed over the period 1965–93. Data have been filtered to remove periods less than 10 yr.

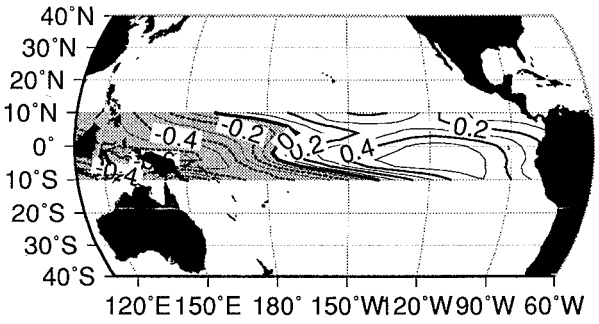

FIG. 19. Correlation between the leading PC of 10–40-yr bandpassed DJF North Pacific SST anomaly and the depth of the 20°C isotherm.

positive τ^x north of 40°N and negative τ^x to the south. As time progresses, this region of positive anomaly slides eastward toward the coast of North America, then abruptly expands across the basin to the west. At the same time, the region of negative anomalies rotates to the north and east. The final effect is that by the time of the last frame (lower right), the situation is reversed from that at the beginning of the sequence.

The variable τ^x was chosen because it plays a role in the connecting the midlatitudes and the Tropics, and close to the equator it has a direct effect in forcing oceanic variability. To show this connection, Fig. 18 presents the simultaneous correlation between the leading PC of low-pass filtered North Pacific SST anomaly (calculated northward of 10°N only) and τ^x, for both the model and observations. The result shows only weak sensitivity to the exact lower-latitude cutoff used, over the range 10°–30°N. Note that, for the observations, the series length (30 yr) is short for considering decadal fluctuations. Wintertime (DJF) values are used, because that is when the North Pacific variability has its clearest expression in SST and sea level pressure (SLP) (Latif and Barnett 1994, 1996); this may be because of the ''Stommel daemon'' effect (Stommel 1979), which has been suggested to be a important part of generating midlatitude variability on decadal timescales (Goodman and Marshall 1999).

In both the model and observations, the region of positive correlation between (decadal timescale) SST anomaly and τ^x extends well into the tropical regions, and has significant expression on the equator. The patterns are different in detail, with the model response being concentrated more toward the western Pacific, but the basic pattern in the Northern Hemisphere is similar. In particular, both the model and observations have a center of divergence/convergence around 130°W on the equator. Together with the τ^x expression in the western Pacific, this suggests that this wind stress pattern could affect the slope of the equatorial thermocline by pumping up in the east and down in the west, or vice versa. Such modulation in the slope of the thermocline could have an effect on the resulting ENSO processes in the ocean, as consistent with the results of Kirtman and Schopf (1998). Note that the relation between the decadal phase and the amplitude of warm/cold events seen in ECHO-2 (Fig. 8) is congruent with this interpretation.

This idea can be tested even more directly by looking at the correlation of the depth of the 20°C isotherm with the same North Pacific SST PC. The result (Fig. 19) shows that indeed the two are correlated in the sense suggested above, such that the overall slope of the thermocline across the basin fluctuates in concert with North Pacific SST anomaly. Vertical excursions in the (yearly averaged) depth of the 20°C isotherm associated with the decadal variability are modest, in the range of ±2 m; however, this is comparable to excursions from ENSO activity, which are about ±5 m in the model.

In sum, data from the ECHO-2 model supports the idea that the near-simultaneous relationships between the midlatitudes and Tropics found on decadal timescales occurs via the intermediary of the atmosphere. Variability in North Pacific SST is strongly related to changes in τ^x that are both local and extend into the

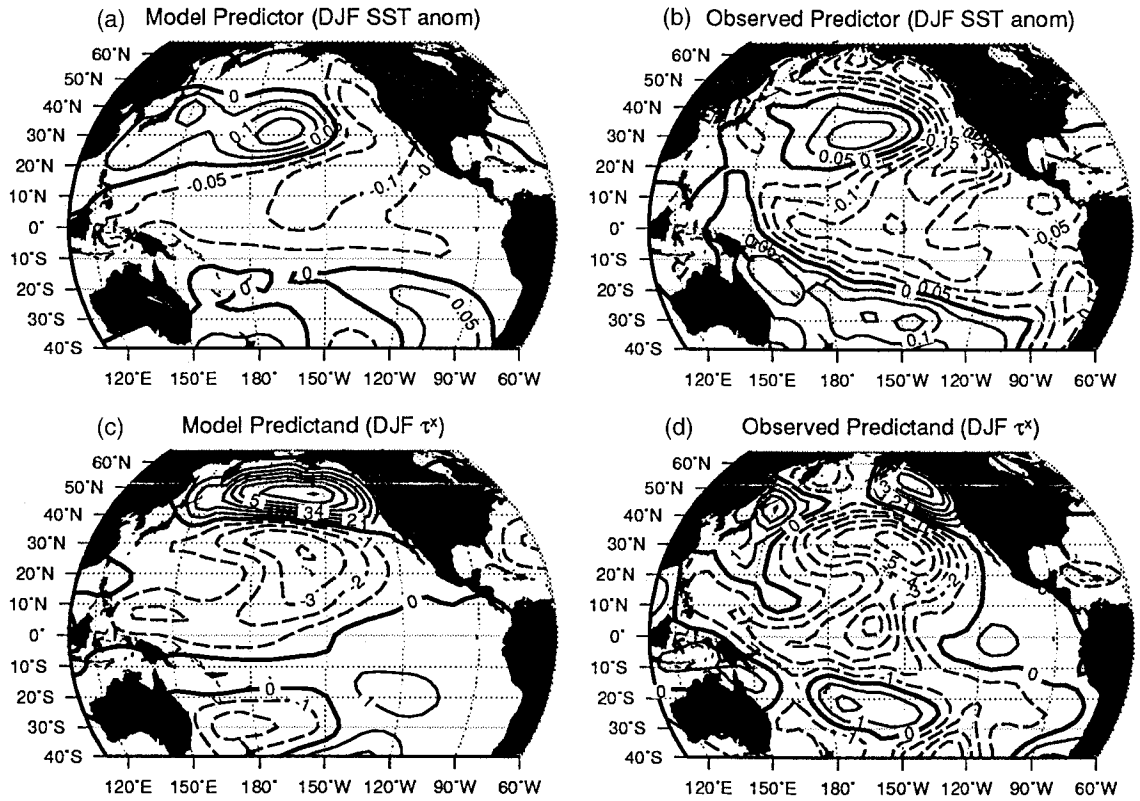

FIG. 20. Canonical correlation analysis of SST anomaly and zonal wind stress anomaly, for both model (left column) and observations over the period 1965–93 (right column). Upper panels show the SST pattern that predicts zonal wind stress (lower panels). Data have been 10–40-yr bandpass filtered.

tropical regions. These changes in τ^x are, in turn, related to changes in the east–west slope of the thermocline across the equator. Since the slope of the equatorial thermocline can affect the ENSO process (Kirtman and Schopf 1998), this leads to a link between decadal-scale midlatitude SST variability and changes in ENSO variability, a link that is borne out in the model (Fig. 8). The question of causality—whether the midlatitudes initiate the change, which is then felt in the Tropics, or vice versa—will be discussed in the next section.

7. Discussion

The results from sections 3–5 show that the strongest link between the Tropics and midlatitudes on decadal timescales is communicated near-simultaneously via changes in surface wind stress. Changes in North Pacific SST are associated with changes in τ^x, which in turn are associated with changes in the east–west slope of the equatorial thermocline. However, this does not establish causality by itself; do the midlatitudes force the Tropics, or vice versa?

This question has been addressed previously when looking at shorter timescale phenomena (Horel and Wallace 1981; Barnett 1981; Hoskins and Karoly 1981), where it is generally found that the Tropics force the midlatitudes. Here, however, we are concerned with timescales of a decade or longer, which those studies did not consider.

To approach this question we performed a canonical correlation analysis (CCA) on DJF data from both the model and observations, using SST as the predictor and τ^x as the predictand. Unlike the correlation map shown in Fig. 18, which was constructed by explicitly choosing a North Pacific SST index to correlate to, the CCA does not impose any preconceived ideas of what or where the relationship should be (beyond the fact that we used 10–40-yr bandpassed data). The result are shown in Fig. 20. The lead predictor, in both the model and observations, is the SST pattern associated with the North Pacific decadal variability. The pattern has weak expression in the Tropics but is clearly a true basinwide pattern with maximum energy in the midlatitudes. The associated pattern of τ^x is similar to Fig. 18, with a strong expression in the central North Pacific and a lobe that reaches to the equator. This suggests the midlatitude decadal SST anomalies, found by Latif and Barnett (1994, 1996) to evolve independently of low-latitude conditions, force a change in the trade wind system that is felt in the Tropics.

Of course, the question of causality cannot be completely answered with an inherently coupled model. Ide-

ally, it would be addressed by regionally altering the coupled GCM's atmosphere–ocean coupling and seeing what effect that has. A similar, but uncoupled, approach was taken by Latif and Barnett (1994), who applied a North Pacific SST anomaly similar to that shown in Fig. 4 as the lower boundary condition to an (albeit different) atmospheric GCM (AGCM). All SSTs south of 20°N were set to zero in the experiment so that there would be no effects from the Tropics. The resultant SLP anomaly was, therefore, clearly produced by extratropical SST and included an expression of τ^x in the western Tropics similar to that found here (Fig. 18), although weaker and different in details. This suggests that the correct interpretation of the CCA analysis is that midlatitude SST anomalies are forcing the τ^x changes that lead to decadal modulation of tropical SST variability.

8. Conclusions

We have investigated the mechanisms connecting the Tropics and midlatitudes in the Pacific basin on decadal timescales using a 137-yr run of a fully coupled ocean–atmosphere general circulation model, ECHO-2, and observations where available. ECHO-2 has some limitations relevant to the question investigated here that should be kept in mind. First, the OGCM's resolution is not sufficient to accurately model coastally trapped waves, which might carry information between the Tropics and midlatitudes in a way that is not accurately simulated in the model. Second, the model's representation of the subpolar gyre is weaker than observed, which should be taken into account when considering the relative roles of the subtropical and subpolar gyres as deduced from these results. Taking these into account, our conclusions are as follows.

1) There are significant correlations between low-frequency activity in the midlatitudes and Tropics, for example, between SST anomalies in the central North Pacific and on the equator. Cold conditions in the central North Pacific are associated with stronger El Niños. There is a less consistent association between warm conditions in the central North Pacific and stronger La Niñas.
2) The correlations between the midlatitudes and Tropics are strongest at time lags of one year or less. Therefore, we conclude that they do not arise from oceanic advection along isopycnals, as that would impose a 7-yr time lag between cause and effect.
3) Midlatitude SST anomalies are strongly correlated with changes in τ^x. The correlation pattern of τ^x includes expression in the Tropics, such as would be associated with a change in the east–west slope of the equatorial thermocline, and is seen in both the model and observations. A direct check shows that midlatitude SST anomalies are correlated with changes in the slope of the equatorial thermocline. We conclude that the near-simultaneous link between the midlatitudes and Tropics is effected via changes in surface wind stress.
4) Results from a canonical correlation analysis of both the model and observations, and previous work forcing an AGCM with a ''Pacific decadal oscillation''-type SST pattern, suggest that the causality is as follows: midlatitude SST anomalies directly force an atmospheric pressure response that includes surface stress anomalies in the equatorial region, thereby forcing changes in the slope of the equatorial thermocline. This provides a mechanism whereby North Pacific processes could modulate the ENSO signal. This causality needs to be confirmed by further numerical experimentation.

Finally, note that the three hypothesis considered here—advection along isopycnals, wave propagation, and atmospheric connections—are not mutually exclusive, and in fact all three are present in the model. Our findings therefore suggest that in a system where all three are operating, and in the presence of realistic levels of decadal midlatitude variability as well as ENSO variability, the atmospheric connection dominates.

Acknowledgments. This work benefited from discussions with Niklas Schneider of Scripps. The authors gratefully acknowledge support from the Department of Energy's CHAMMP Program (DE-FG03-91-ER61215), the National Science Foundation (NSF ATM-93-14495), the Scripps Institution of Oceanography, the Max Planck Institute for Meteorology, and the European Union's SYNTEX Programme. The simulations were executed at NCAR's Climate Simulation Laboratory (CSL) by J. Ritchie; we especially appreciate the help provided by CSL personnel.

APPENDIX

Climatology of ECHO-2

In this appendix are presented some selected illustrations of the ECHO-2 climatology for the Pacific ocean, the region of interest here. Other information can be found in Frey et al. (1997), who present, for the tropical Pacific, ECHO-2's annual mean fields for SST, precipitation, net surface heat flux, zonal and meridional wind stress, and net surface solar radiation, as well as equatorial sections of temperature and zonal currents.

a. Currents and streamfunction

A vertical section of zonal currents along the equator is shown in Frey et al. 1997. Here, we show time-averaged velocity vectors at 15-m depth (Fig. A1) for the ECHO-2 model, and from observations (Reverdin et al. 1994) over the period 1987–92. The large-scale pattern of tropical currents in ECHO-2 is similar to that observed. The westward-flowing South Equatorial Current (SEC) extends from about 3°N to 8°S, with a distinct

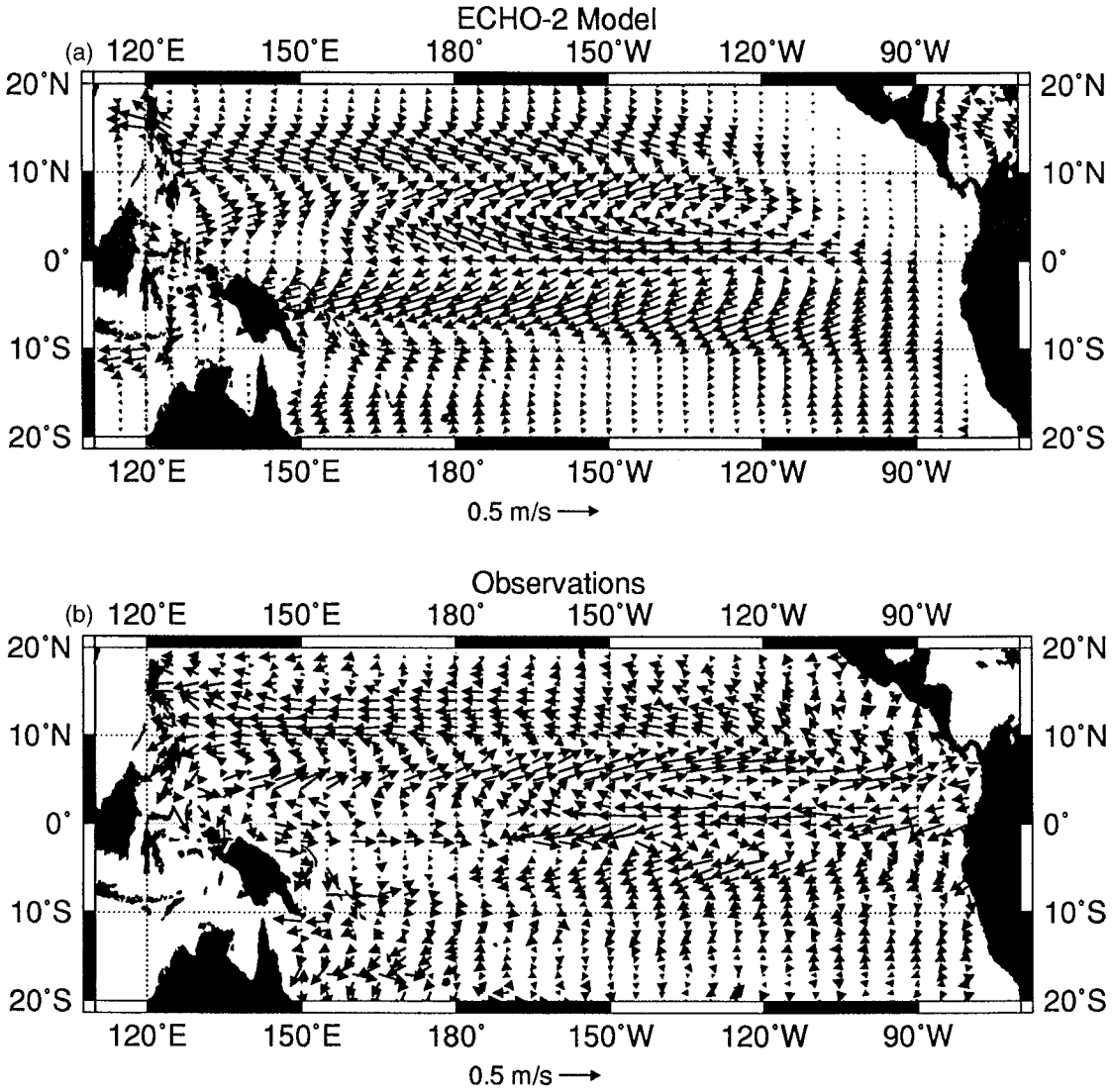

FIG. A1. Velocity vectors at 15 m from (a) ECHO-2 and (b) observations (from Reverdin et al. 1994) over the period 1987–92.

minimum on the equator and currents in the range of 0.5 to 0.6 m s^{-1}, somewhat stronger than those observed (0.4 to 0.5 m s^{-1}). The model's SEC extends too far to the southwest compared to the observations, however; possibly this is related to flow associated with the cold tongue, which extends too far to the west in the model. A South Equatorial Countercurrent can be seen in ECHO-2 at about 10°S, but only rather indistinctly in the observations. In ECHO-2, the North Equatorial Countercurrent (NECC) extends from about 4°N, 130°E to 8°N, 110°W, with peak velocities of about 0.35 m s^{-1}. This is comparable in strength to the observations, which also have peak velocities of about 0.35 m s^{-1}, but the NECC does not penetrate as far to the east in the model (110°W) as it does in observations (90°W). The model's North Equatorial Current extends from about 10° to 14°N, with peak currents of 0.3 to 0.4 m s^{-1}, again somewhat stronger than those observed (about 0.25 m s^{-1}).

The time-averaged mass transport streamfunction is shown in Fig. A2. Transport in the Kuroshio is about 45 Sv (Sv $\equiv 10^6$ m^3 s^{-1}) on average, in good agreement with observed values, which suggests a transport that varies seasonally between 38.5 and 46.5 Sv (Taft 1972). The subpolar gyre, however, is distinctly underrepresented, with typical transports of 2–4 Sv.

b. Sea surface height

Time-average SSH for ECHO-2 is shown in Fig. A3, along with that observed by TOPEX over the period October 1992 to February 1995. (An offset of 1.0 m has been added to the ECHO-2 data to make the zero lines similar in ECHO-2 and the observations, for easier

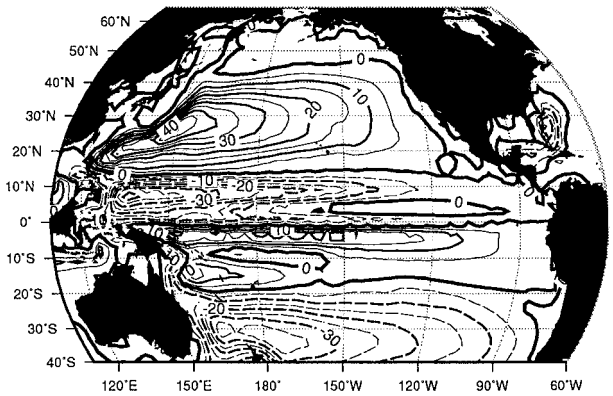

FIG. A2. Mass transport streamfunction for the ECHO-2 model. Contour interval is 5×10^6 m^3 s^{-1}.

comparison.) The features associated with the tropical current system are clearer in ECHO-2 than in the observed dataset, although note the short time period of the observations (29 months). The sea level drop across the model's western boundary current region is about 0.8 m, similar to that seen in the TOPEX data. Also,

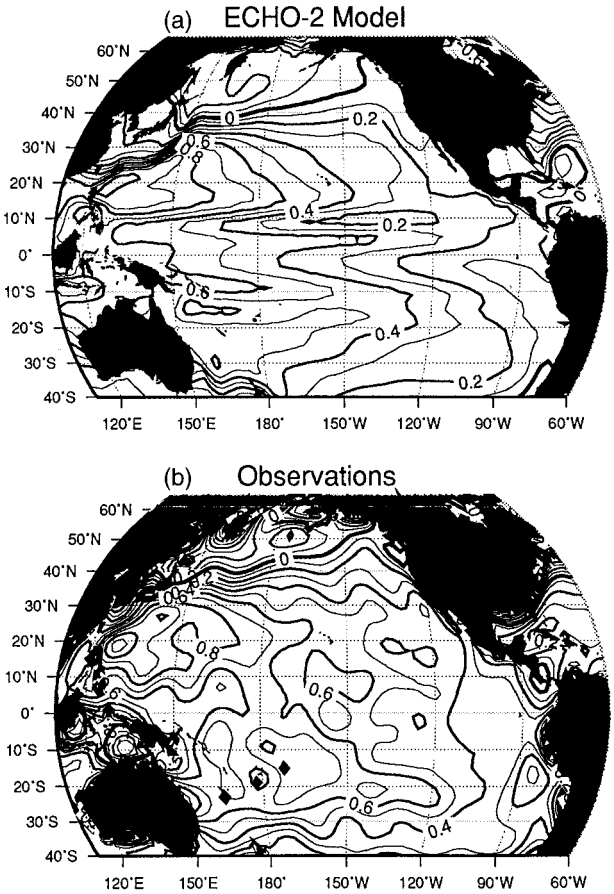

FIG. A3. Contours of mean sea surface height for (a) ECHO-2 and (b) observed from TOPEX over the period October 1992 to February 1995. Contour interval is 0.1 m.

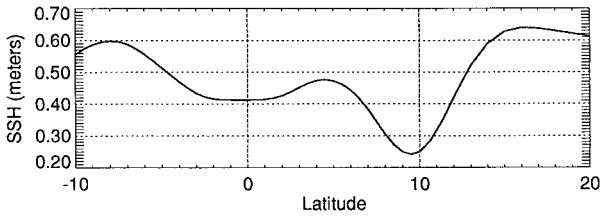

FIG. A4. Section of sea surface height along the date line for the ECHO-2 model.

the sea level difference between the eastern and western Pacific is similar in ECHO-2 (0.5 m) to the observations (0.5 m), although the slope is more regular in ECHO-2. Note, however, that the subpolar gyre is poorly represented in the model, with a relatively bland SSH field in the northwest Pacific with minimum of about −0.2 m, versus twice that in the observations.

A section of SSH along the dateline is shown in Fig. A4. The local minimum at the equator, associated with divergent flow in the meridional plane, can be seen along with the local maximum at 5°N associated with convergent meridional flow. The slope down to the minimum at 9°N, associated with the NECC, is clearly distinguishable.

c. Temperature transect

Figure A5 shows time-averaged temperature along the date line from the ECHO-2 model and observations (Levitus 1994). The temperature structure in the subpolar North Pacific north of 35°N is suggestive of too

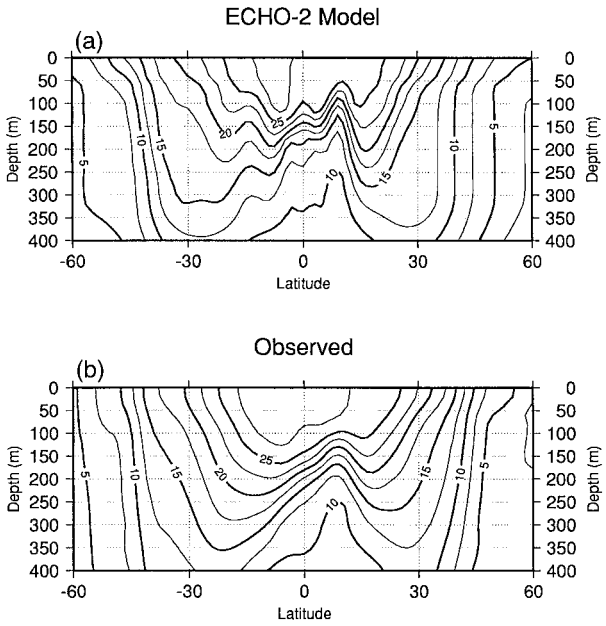

FIG. A5. Time-average temperature along the date line (a) from the ECHO-2 coupled model and (b) observations (Levitus 1994). Contour interval is 2.5°C.

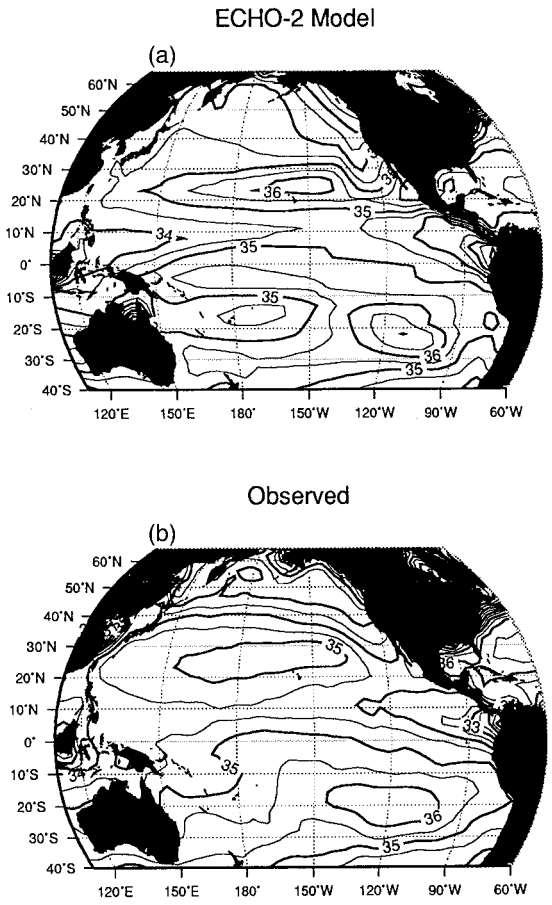

FIG. A6. Surface time average salinity from (a) the ECHO-2 coupled model and (b) observations (Levitus 1994). Contour interval is 0.5 psu.

much vertical mixing, but the structure near the equator, including an upward lifting of the isotherms near 10°N and the vertical spreading of the isotherms on the equator, is similar to that observed. Note that both the observations and the ECHO-2 data are averages over long time intervals, which will tend to blur finescale features.

d. Salinity

Figure A6 shows average surface salinity from the ECHO-2 run and from observations (Levitus 1994), for comparison. Salinities tend to be elevated in the model, especially in the subpolar North Pacific north of 40°N, where the halocline is weaker than observed. This can be seen in Fig. A7 as well, which shows a transect along the date line using the same datasets. Increased vertical mixing, which could reasonably be expected to go with the reduced halocline in ECHO-2, might downplay the importance of the subpolar gyre in the model results presented here, as compared to the real oceans.

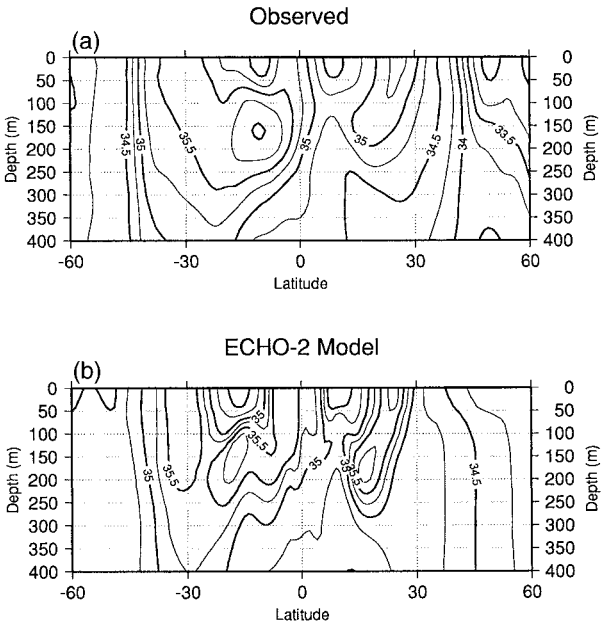

FIG. A7. Time-average salinity along the dateline from (a) the ECHO-2 coupled model and (b) observations (Levitus 1994). Contour interval is 0.25 psu.

e. Mixed layer depth

Climatological mixed layer depth in the central North Pacific, averaged over the region 30°–40°N, 160°E–160°W is shown in Fig. A8. Also shown are observed values from the Integrated Global Ocean Services (IGOSS) mixed layer depth climatology, which was formed from analysis of the Naval Oceanographic Data Center (NODC) Global Ocean Temperature/Salinity dataset over the period 1955 to 1988 and the Global Temperature–Salinity Pilot Project dataset over the years 1989 to 1994. The phasing of ECHO-2's response, as well as the summer and autumn depths, are similar to observed, but the winter–early spring values in ECHO-2

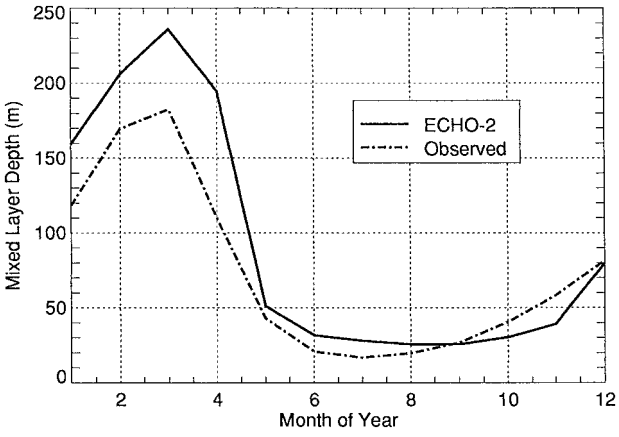

FIG. A8. Climatological mixed layer depth in the central North Pacific for ECHO-2 (solid) and observations (dashed).

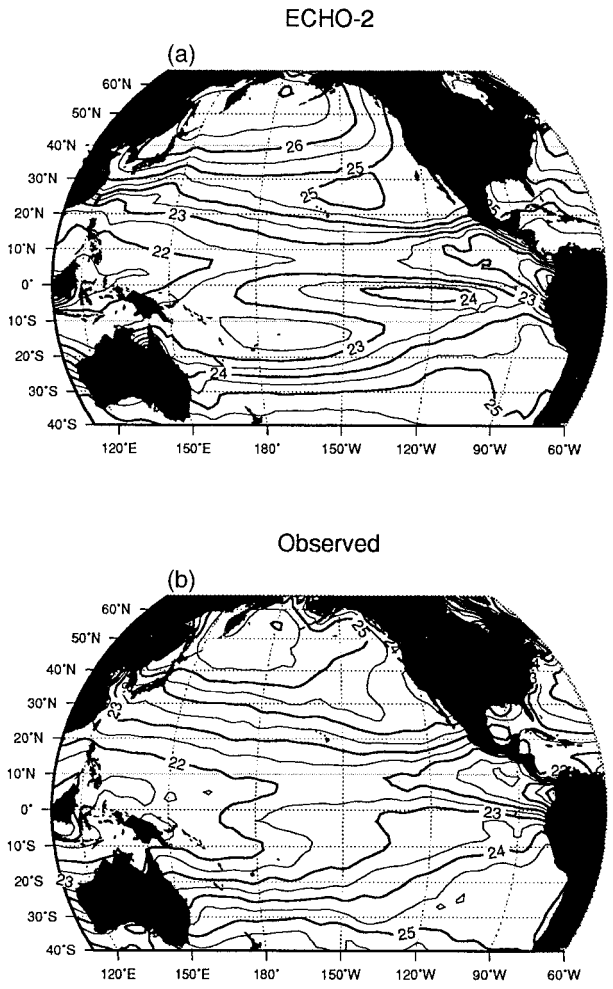

FIG. A9. Time-averaged density at 10 m for (a) ECHO-2 and (b) from observations. Contour interval is 0.5 σ_θ units.

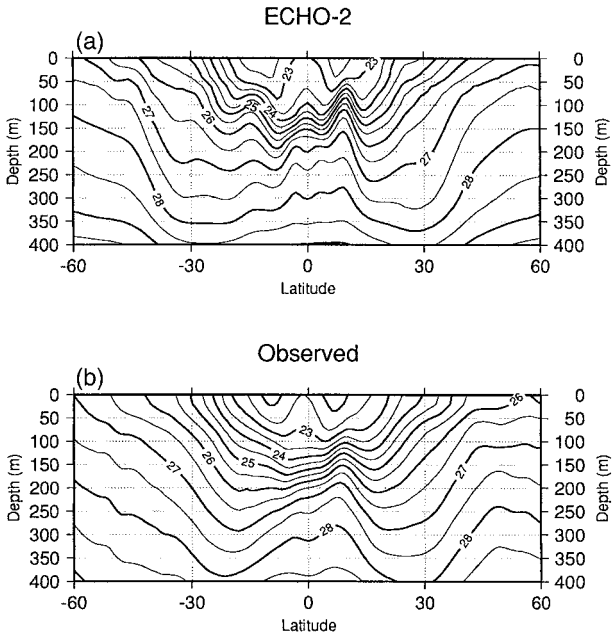

FIG. A10. Transect of density along the date line for (a) ECHO-2 and calculated from (b) observed temperature and salinity (Levitus 1994). Contour interval is 0.5 σ_θ units.

are typically 50 m too deep. In the context of section 4, which explores the implications of propagation of thermal anomalies along isopycnal layers from midlatitude source regions to the Tropics, this suggests that ECHO-2's deeper ventilation might insert a midlatitude signal into a somewhat greater range of isopycnals, possibly opening up additional propagation paths between the model's midlatitudes and Tropics that do not exist in nature.

f. Density structure

Density at 10 m is shown in Fig. A9 for ECHO-2 and calculated from observations (Levitus 1994). Model values in the western Pacific are about 22 σ_θ units, similar to that observed. In the model, densities ramp up to 25 σ_θ units between 30° and 35°N, about 5° south of where they reach that value in the observations. The subpolar gyre is too dense, with values of about 26.5 σ_θ units compared to 25.5 σ_θ units in the observations. Similarly, the equatorial cold tongue is too strong, reaching 24 σ_θ units versus 23.5 in the observations. In the South Pacific the agreement is good, with model values increasing from 23 σ_θ units at about 21°S (vs 20°S in the observations) to a value of 25 σ_θ units at 30°S (approximately the same latitude as observed). A region with uniform density of between 24.5 and 25 σ_θ units off the coast of Chile is well reproduced by the model, as is a wedge of low-density water, bounded by fronts on the north and south, that extends out from the west coast of Central America.

A transect of density along the date line is shown in Fig. A10. The undulations in the density surfaces in ECHO-2 are similar to the observations, with a distinct bowl shape in subtropical latitudes and a pronounced ridge at about 10°N, but the surfaces tend to be about 50 m too shallow in the model. Comparing this to the previous figures of salinity and temperature transects along the date line, this can be seen to be due to generally elevated salinity in the ECHO-2 run, which is more pronounced in the Northern Hemisphere than the Southern Hemisphere.

g. Hindcast SST

Because the mixing parameterization of the ocean model component of a coupled ocean–atmosphere GCM must be tuned, the question can arise whether this tuning has skewed the ocean model to produce apparently realistic SST values—but with an incorrect balance of processes—in order to compensate for systematic deficiencies in the atmospheric component. While it is difficult to answer this question definitively, a straight-

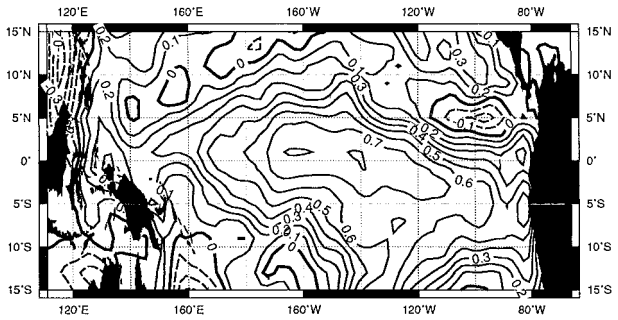

FIG. A11. Correlation between observed and ocean model *only* SST anomalies, where the ocean model was forced by observed wind stresses over the period 1970–85.

forward check is to test the quality of the tuned ocean model by itself when forced by observed fields. It could reasonably be supposed that tuning the ocean component into an unrelistic mixing regime in order to compensate for systematic AGCM biases would degrade the quality of an ocean-only simulation. Figure A11 shows the results of such a test, in which the OGCM is forced only with observed Florida State University winds (Goldenberg and O'Brien 1981) over the period 1970–85, and the model-evolved SST anomalies are compared to those observed over the same period. This particular test is chosen for two reasons: 1) a comparison with other models is available in Miller et al. (1993), whose procedures described therein were followed here; and 2) tropical SSTs are sensitive to a variety of effects, including vertical and horizontal mixing (Barnett et al. 1993) and equatorial wave processes (Philander 1990), which must therefore be correctly represented for a good result. Figure A11 shows that the OGCM component evolves SST anomalies that correlate to those observed at values greater than 0.7 over a range of the Tropics from about 110° to 170°W, with peaks of greater than 0.8 correlation. Computing to Miller et al.'s results, by this particular measure the OGCM used here is entirely comparable to the best models tested there. Note that no midlatitude SST response is expected in this test case with wind stress forcing only.

REFERENCES

Alexander, M. A., 1992: Midlatitude atmosphere–ocean interaction during El Nino. I. The North Pacific Ocean. *J. Climate,* **5,** 944–958.

——, and C. Deser, 1995: A mechanism for the recurrence of wintertime midlatitude SST anomalies. *J. Phys. Oceanogr.,* **25,** 122–137.

Barnett, T. P., 1981: Statistical prediction of North American air temperatures from Pacific predictors. *Mon. Wea. Rev.,* **109,** 1021–1041.

——, M. Latif, N. Graham, M. Flugel, S. Pazan, and W. White, 1993: ENSO and ENSO-related predictability. Part I: Predictions of equatorial Pacific sea surface temperature with a hybrid coupled ocean–atmosphere model. *J. Climate,* **6,** 1545–1566.

——, D. W. Pierce, M. Latif, D. Dommenget, and R. Saravanan, 1999: Interdecadal interactions between the tropics and midlatitudes in the Pacific basin. *Geophys. Res. Lett.,* **26,** 615–618.

Blackmon, M. L., J. E. Geisler, and E. J. Pitcher, 1983: A general circulation model study of January climate anomaly patterns associated with interannual variation of equatorial Pacific sea surface temperatures. *J. Atmos. Sci.,* **40,** 1410–1425.

da Silva, A. M., C. C. Young, and S. Levitus, 1995: *Atlas of Surface Marine Data 1994.* Vol. 1, *Algorithms and Procedures,* NOAA Atlas NESDIS 6, 299 pp.

Deser, C. M., A. Alexander, and M. S. Timlin, 1996: Upper-ocean thermal variations in the North Pacific during 1970–1991. *J. Climate,* **9,** 1840–1855.

Enfield, D. B., and J. S. Allen, 1980: On the structure and dynamics of monthly mean sea level anomalies along the Pacific coast of North and South America. *J. Phys. Oceanogr.,* **10,** 557–578.

Fine, R. A., W. H. Peterson, and H. G. Ostlund, 1987: The penetration of tritium into the tropical Pacific. *J. Phys. Oceanogr.,* **17,** 553–564.

Frey, H., M. Latif, and T. Stockdale, 1997: The coupled GCM ECHO-2. Part I: The tropical Pacific. *Mon. Wea. Rev.,* **125,** 703–720.

Gill, A. E., 1982: *Atmosphere–Ocean Dynamics.* Academic Press, 662 pp.

Goddard, L., and N. E. Graham, 1997: El Nino in the 1990s. *J. Geophys. Res.,* **102,** 10 423–10 436.

Goldenberg, S. B., and J. J. O'Brien, 1981: Time and space variability of tropical Pacific wind stress. *J. Phys. Oceanogr.,* **11,** 1190–1207.

Goodman, J., and J. Marshall, 1999: A model of decadal middle-latitude atmosphere–ocean coupled modes. *J. Climate,* **12,** 621–641.

Graham, N. E., 1994: Decadal-scale climate variability in the tropical and North Pacific during the 1970's and 1980's: Observations and model results. *Climate Dyn.,* **10,** 135–162.

Gu, D., and S. G. H. Philander, 1997: Interdecadal climate fluctuations that depend on exchanges between the tropics and extratropics. *Science,* **275,** 805–807.

Horel, J. D., and J. M. Wallace, 1981: Planetary-scale atmospheric phenomena associated with the Southern Oscillation. *Mon. Wea. Rev.,* **109,** 813–829.

Hoskins, B. J., and D. J. Karoly, 1981: The steady linear response of a spherical atmosphere to thermal and orographic forcing. *J. Atmos. Sci.,* **38,** 1179–1196.

Kirtman, B. P., and P. S. Schopf, 1998: Decadal variability in ENSO predictability and prediction. *J. Climate,* **11,** 2804–2822.

Latif, M., and T. P. Barnett, 1994: Causes of decadal climate variability over the North Pacific and North America. *Science,* **266,** 634–637.

——, and ——, 1996: Decadal climate variability over the North Pacific and North America: Dynamics and predictability. *J. Climate,* **9,** 2407–2423.

Levitus, S., 1994: *World Ocean Atlas 1994.* U.S. Dept. of Commerce, 552 pp.

Liu, Z., and S. G. H. Philander, 1995: How different wind stress patterns affect the tropical–subtropical circulations of the upper ocean. *J. Phys. Oceanogr.,* **25,** 449–462.

Lu, P., and J. P. McCreary, 1995: Influence of the ITCZ on the flow of thermocline water from the subtropical to the equatorial Pacific Ocean. *J. Phys. Oceanogr.,* **25,** 3076–3088.

Luyten, J. R., J. Pedlosky, and H. Stommel, 1983: The ventilated thermocline. *J. Phys. Oceanogr.,* **13,** 292–309.

Lysne, J., P. Chang, and B. Giese, 1997: Impact of the extratropical Pacific on equatorial variability. *Geophys. Res. Lett.,* **24,** 2589–2592.

McCreary, J. P., and P. Lu, 1994: Interaction between the subtropical and equatorial ocean circulations: The subtropical cell. *J. Phys. Oceanogr.,* **24,** 466–497.

McPhaden, M. J., and R. A. Fine, 1988: A dynamical interpretation of the tritium maximum in the central equatorial Pacific. *J. Phys. Oceanogr.,* **18,** 1454–1457.

Mechoso, C. R., and Coauthors, 1995: The seasonal cycle over the tropical Pacific in coupled ocean–atmosphere general circulation models. *Mon. Wea. Rev.,* **123,** 2825–2838.

Miller, A. J., T. P. Barnett, and N. E. Graham, 1993: A comparison of some tropical ocean models: Hindcast skill and El Niño evolution. *J. Phys. Oceanogr.,* **23,** 1567–1591.

——, W. B. White, and D. R. Cayan, 1997: North Pacific thermocline variations on ENSO timescales. *J. Phys. Oceanogr.,* **27,** 2023–2039.

Namias, J., 1969: Seasonal interactions between the north Pacific Ocean and the atmosphere during the 1960s. *Mon. Wea. Rev.,* **97,** 173–192.

——, X. Yuan, and D. R. Cayan, 1988: Persistence of North Pacific sea surface temperature and atmospheric flow patterns. *J. Climate,* **1,** 682–703.

Nitta, T., and S. Yamada, 1989: Recent warming of tropical sea surface temperature and its relationship to the Northern Hemisphere circulation. *J. Meteor. Soc. Japan,* **67,** 375–383.

Philander, S. G., 1990: *El Nino, La Nina, and the Southern Oscillation.* Academic Press, 293 pp.

Press, W. H., B. P. Flannery, S. A. Teukolsky, and W. T. Vetterling, 1989: *Numerical Recipes*. Cambridge University Press, 702 pp.

Reverdin, G., C. Frankignoul, E. Kestenare, and M. McPhaden, 1994: Seasonal variability in the surface currents of the equatorial Pacific. *J. Geophys. Res.,* **99,** 20 323–20 344.

Roeckner, E., and Coauthors, 1996: The Atmospheric General Circulation Model ECHAM-4: Model description and simulation of present-day climate. Tech. Rep. 218, 90 pp. [Available from DKRZ, Bundesstr. 55, 20146, Hamburg, Germany.]

Schneider, N., and T. P. Barnett, 1997: The Indonesian throughflow in a coupled GCM. *J. Geophys. Res.,* **102,** 12 341–12 358.

——, A. J. Miller, M. A. Alexander, and C. Deser, 1999: Subduction of decadal North Pacific temperature anomalies: Observations and dynamics. *J. Phys. Oceanogr.,* **29,** 1056–1070.

Stommel, H., 1979: Determination of water mass properties of water pumped down from the Ekman layer to the geostrophic flow below. *Proc. Natl. Acad. Sci.,* **76,** 3051–3055.

Taft, B. A., 1972: Characteristics of the flow of the Kuroshio south of Japan. *Kuroshio: Physical Aspects of the Japan Current,* H. Stommel, Ed., University of Washington Press, 165–216.

Trenberth, K. E., 1990: Recent observed interdecadal climate changes in the Northern Hemisphere. *Bull. Amer. Meteor. Soc.*, **71,** 988–993.

——, and J. W. Hurrell, 1994: Decadal atmosphere-ocean variations in the Pacific. *Climate Dyn.,* **9,** 303–319.

Venzke, S., M. Latif, and A. Villwock, 2000: The Coupled GCM ECHO-2. Part II: Indian Ocean response to ENSO. *J. Climate,* **13,** 1371–1383.

Wang, B., 1995: Interdecadal changes in El Niño onset in the last four decades. *J. Climate,* **8,** 267–285.

Wolff, J.-O., E. Maier-Reimer, and S. Legutke, 1997: HOPE, The Hamburg Ocean Primitive Equation Model. Tech. Rep. DKRZ-TR-13, 113 pp. [Available from DKRZ, Bundesstr. 55, 20146, Hamburg, Germany.]

Zhang, Y., J. M. Wallace, and D. S. Battisti, 1997: ENSO-like interdecadal varaibility: 1900–93. *J. Climate,* **10,** 1004–1020.